Spring 1-1-2012

Impact of Temperature Cycles on the Thermal Consolidation of Saturated Silt Under Different Stress States

Alexander Vega
University of Colorado at Boulder, alexander.vega@colorado.edu

IMPACT OF TEMPERATURE CYCLES ON THE THERMAL CONSOLIDATION OF SATURATED SILT UNDER DIFFERENT STRESS STATES

by

Alexander Vega

B.S., Colorado State University-Pueblo

A thesis submitted to the

Faculty of the Graduate School of the

University of Colorado in partial fulfillment

of the requirement for the degree of

Master of Science

Department of Civil, Environmental, and Architectural Engineering

2012

Impact of Temperature Cycles

on the Thermal Consolidation of Saturated Silt

under Different Stress States

written by Alexander Vega

has been approved by the Department of Civil, Environmental, and Architectural Engineering

_____

Professor John McCartney (committee chair)

_____

Professor Dobroslav Znidarčić

_____

Professor Shideh Dashti

Date_____

The final copy of this thesis has been examined by the signatories, and we find that both the content and the form meet the acceptable presentation standards of scholarly work in the above mentioned discipline.

Alexander Vega (M.S. Civil Engineering, Department of Civil, Environmental, and Architectural Engineering)

Impact of Temperature Cycles on the Thermal Consolidation of Saturated Silt under Different Stress States

Thesis directed by Professor John S. McCartney

ABSTRACT

Ground-source heat pumps (GSHPs) are a well-established approach to provide energy-efficient heating and cooling to buildings by exchanging heat with the subsurface soil or rock, which has a relatively constant temperature compared to that of the outside air. Although heating and cooling of the ground may lead to thermally-induced volume change in the soil surrounding the heat exchanger, this is typically ignored in the analysis and design of these systems. This is not the case when heat exchangers are embedded within the foundations of buildings to form "energy foundations". In this case, temperature fluctuations within the foundation during typical heat exchange operations may lead to permanent thermal-induced volume changes in the soil which may affect the performance of the foundation and overlying structure. The objective of this study is to understand the impact of cyclic heating and cooling on the thermally induced volume change of soils, as a first step in understanding the expected long-term deformation behavior of energy foundations. Although thermo-elasto-plastic theories of thermal consolidation in the literature indicate that permanent, plastic volume change should only occur on the first heating cycle, some data in the literature indicates additional permanent volume changes may be encountered on subsequent cycles.

This study is focused on the thermal volume change behavior of compacted, saturated silt, under different stress states. Specifically, a temperature-regulated oedometer with back-

pressure control is used to measure the temperature-axial strain behavior of silt under normally consolidated to heavily-overconsolidated stress states. During the first cycle of heating, the silt specimens were observed to have thermal volume changes that were similar to those reported in the technical literature, with the normally consolidated specimen showing contraction and the overconsolidated specimens showing expansion during heating. The specimens all showed contraction during cooling as expected. However, on subsequent heating and cooling cycles, all of the specimens were observed to show a small amount of cumulative contraction. This behavior contradicts the theories of thermal volume change in soils in the literature which indicate that the volume change on subsequent heating and cooling cycles should be elastic. This cumulative contraction was observed in the results even though a stiffer response was expected due to differential radial expansion of the oedometer ring during heating and cooling. Further, thermally induced pore water pressures were observed on each heating cycle, with the magnitude of the change in pore water pressure decreasing after each cycle. Although the results from this study provide data that may be used to improve the theories for thermo-elasto-plastic thermal volume change mechanisms in soils, testing of other soil types is necessary for these conclusions to apply more broadly.

ACKNOWLEDGEMENT

The author wishes to thank his advisor, Professor John Scott McCartney, for his guidance, assistance, and positive attitude, which helped immensely through the completion project. Special recognition is given to Professors Dobroslav Znidarcic and Shideh Dashti for serving as part of my thesis committee. Deserving of additional thanks for their enthusiasm and assistance are the many geotechnical engineering students and professors at the University of Colorado Boulder, whom there are far too many to list. A special thanks goes to Wendy, Alessandra, and my family, who have inspired me to achieve my goals. Funding from NSF grant CMMI 0928159 is greatly appreciated.

Table of Contents

List of Tables

List of Figures

1. INTRODUCTION

1.1. Motivation

Ground-source heat pumps (GSHPs) are a well-established approach to provide energy efficient heating and cooling to buildings by exchanging heat with the subsurface soil or rock, which has a relatively constant temperature compared to that of the outside air. Although heating and cooling of the ground may lead to thermally-induced volume change in the soil surrounding the heat exchanger, this is typically ignored in the analysis and design of these systems. This is not the case when heat exchangers are embedded within the foundations of buildings to form "energy foundations". In this case, temperature fluctuations within the foundation during typical heat exchange operations may lead to permanent thermal-induced volume changes in the soil that may affect the performance of the foundation and overlying structure. An understanding of the mechanisms of thermal volume change of soils under different stress states may help improve the interpretation of strain measurements from energy foundations during heating and cooling operations. In particular, the impact of temperature cycles on soil volume change is particularly important to understand because energy foundations experience relatively slow fluctuations in temperature over time due to heating and cooling demands from the building, with temperatures ranging from 3 to 35 °C (Omer 2008; Murphy and McCartney 2012).

1.2. Problem Statement

Contradictory conclusions regarding the impact of temperature cycles on the thermal volume change of soils have been published in the literature. One of the earliest papers to investigate the impact of heating and cooling cycles on the thermal volume change of soils was performed by Campanella and Mitchell (1968). They observed that a saturated specimen of normally consolidated Illite clay showed a large contraction during the first stage of heating, followed by

additional contraction during cooling, as shown in Figure 1.1(a). This change in volume corresponds with drainage of water from the soil specimen due to greater thermal expansion of the pore water compared to the soil grains. During subsequent heating and cooling cycles, a smaller amount of additional contraction was observed. The behavior observed during these subsequent heating and cooling cycles was not thoroughly explained by Campanella and Mitchell (1968). Further, these results cannot be explained using current thermo-elasto-plastic models. The components of elastic and plastic thermal volumetric strains during a heating and cooling cycle predicted by the model of Cui et al. (2000), which is based upon an earlier model developed by Huekel and Borsetto (1990), are shown in Figure 1.1(b). The elastic thermal strain should be expansive, while the plastic thermal strain is contractive. The basis of these models is that plastic thermal strains should only occur on the first heating cycle of normally consolidated clay. After the initial heating cycle, all thermal strains should be elastic and expansive up to the previous temperature applied because they fall under a thermal yield surface. The cyclic effects in Figure 1.1(a) deserve further experimental evaluation.

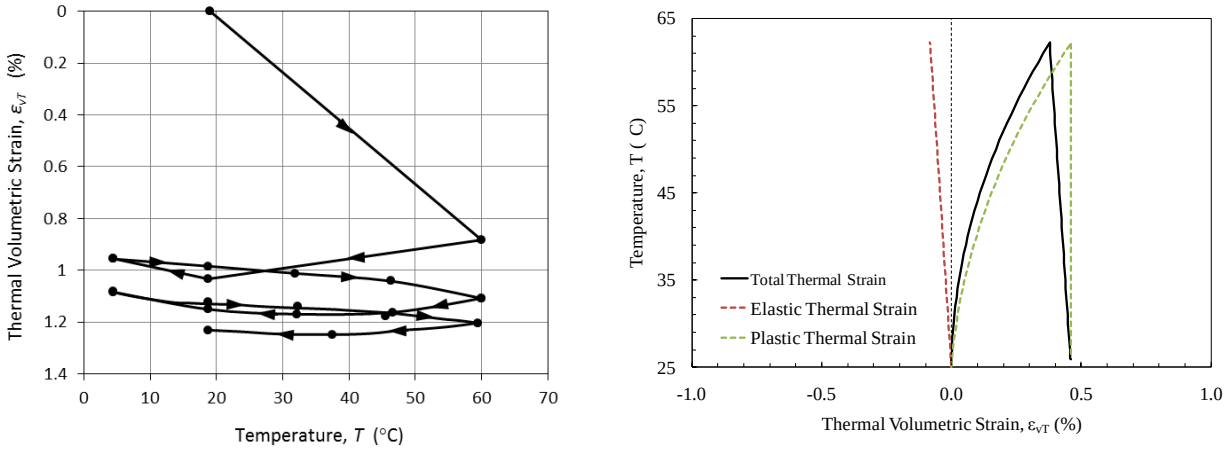

(a) (b)

Figure 1.1: Contradicting conclusions on thermal volume change of saturated soils: (a) Thermal volume change results for saturated, normally consolidated Illite clay under three heating cycles (Campanella and Mitchell 1968); (b) Thermo-elasto-plastic strain volumetric components during a heating cycle from the model of Cui et al. (2000)

1.3. Objectives and Approach

The objective of this study is to understand the impact of cyclic heating and cooling on the thermally induced volume change of soils, as a first step in understanding the expected long-term deformation behavior of energy foundations. Although thermo-elasto-plastic theories of thermal consolidation in the literature indicate that permanent, plastic volume change should only occur on the first heating cycle, data in the literature indicates additional permanent volume changes may be encountered on subsequent cycles. Accordingly, the approach used in this study is to extend the database of thermal volume change measurements by performing a series of thermal consolidation tests on saturated, compacted silt specimens under different stress states. The rationale for investigating different stress states is that many studies have observed that the plastic thermal volume contraction only occurs for normally consolidated and lightly overconsolidated soils (Baldi et al. 1991; Laloui and Cekeravac 2003; Cekeravac and Laloui 2004). Campanella and Mitchell (1968) only investigated the role of temperature cycles for normally consolidated clay, so evaluating whether or not additional thermal volume change occurs during temperature cycles for overconsolidated clays is also important when considering which features of thermo-elasto-plastic models should be enhanced in the future.

1.4. Scope

Chapter 2 includes a review of the mechanisms of thermally-induced volume change, including a more in-depth discussion of the results from Campanella and Mitchell (1968). Chapter 3 presents the geotechnical properties of the silt used in the experimental portion of this study. Chapter 4 includes a description of the experimental setup, including significant that which were implemented to understand the thermo-mechanical machine deflections. Chapter 5 presents the experimental procedures for the tests, including the initial mechanical loading of the

specimens and the application of subsequent heating and cooling cycles. Chapter 6 includes a summary of the results from cyclic thermal consolidation tests on five silt specimens, each which have an increasing overconsolidation ratio (OCR). An analysis of the results is presented in Chapter 7, including plots of the thermal strain as a function of temperature and an assessment of the role of machine deflections in the results. The conclusions of this study are summarized in Chapter 8.

2. LITERATURE REVIEW

2.1. Introduction

The motivation for early studies on the effect of temperature on soil behavior was to understand the impact of temperature changes on soil samples during sampling, storage, and transportation to the laboratory to predict disturbance effects. Consequently, most of the early research efforts concentrated on investigating the behavior of soils under a temperature range up to 30 to 50 °C **(**Gray 1936; Finn 1951; Paaswell 1967; Campanella and Mitchell 1968; Plum and Esrig 1969). Due to different practical applications that arose over time, researchers started to evaluate the behavior of soils under higher temperatures. These include understanding the behavior of soil surrounding buried high-voltage electric cables (Abdel-Hadi and Mitchell 1981) and heated oil and gas pipelines near power plants (Slegel and Davis 1977), both of which experience temperatures in excess of 60 °C. The disposal of nuclear waste in offshore soft clay deposits was another topic of interest (McGinley 1983; Houston et al. 1985). More recently, concerns regarding the thermal response of clay barriers containing nuclear waste prompted further research into studying the behavior of soils under high temperatures (Baldi et al. 1988). The studies on clay barriers and nuclear waste disposal prompted the development of constitutive relationships to predict thermally induced volume changes of soils noted in previous experimental studies (Huekel and Borsetto 1990; Cui et al. 2000). In this regard, extensive studies have been completed using different types of saturated fine-grained soils to investigate their response to the combined effects of stress and temperature (Demars and Charles 1982; Hueckel and Baldi 1990; Towhata et al. 1993; Burghignoli et al. 2000; Sultan et al. 2002; and Cekerevac and Laloui 2004). Recent interest in building heating energy efficiency technologies has continued to drive the interest in the temperature effects on soils. Thermally active

geotechnical systems, including energy foundations, have the unique aspect that they undergo cycles of heating and cooling over time, which differs from the temperature conditions in the previous applications under investigation (Brandl 2006).

The main purpose of this chapter is to review the mechanisms of thermal-induced volume change, the experimental observations of stress history on thermally induced volume changes, and the effects of rate of heating, and effects of temperature cycles on the thermal consolidation of soil. This chapter will include an assessment of the experiments and observations made by several researches using various soils types.

2.2 Mechanisms of Temperature-Induced Volume Change

Prior to discussing the experiments and observations from the literature, the physical mechanisms associated with thermally-induced volume change will be discussed. The thermally-induced volume change in saturated soils in drained conditions has been linked to three different mechanisms described by Paaswell (1967) and Campanella and Mitchell (1968). These mechanisms may result in elastic or plastic volume changes in a soil during heating. This behavior is attributed to the elastic expansion and contraction of the soil and pore water within its matrix. For a soil mass with grains in contact, assuming the same coefficients of thermal expansion for all the soil grains, the thermal volumetric strain can be defined using the coefficient of elastic thermal expansion of the material, as follows:

$$\Delta\varepsilon_{v,T}^{e} = \alpha\Delta T \qquad \text{(Eq. 2.1)}$$

where $\varepsilon_{v,T}^{e}$ is the elastic volumetric thermal strain, α is the coefficient of volumetric thermal expansion for a given material, and ΔT is the temperature change. To be consistent with soil geotechnical engineering conventions, thermal expansion is defined as having a negative sign. This implies that the magnitude of α should be less than zero as ΔT is always positive.

The first mechanism of volume change in saturated soils, described by Campanella and Mitchell (1968), occurs due to differential expansion between the soil particles and water in the pores. When the temperature is increase rapidly, a differential expansion occurs because of greater volumetric expansion of the pore water than of the soil skeleton. Typical coefficients of linear thermal expansion for water and various soil minerals are summarized in Table 2.1. In general, water will expand around 7 times more than that of the soil solids (Sultan et al. 2002).

Table 2.1: Linear coefficients of thermal expansion of water and soil minerals and rocks

Material	Coefficient of Linear Thermal Expansion, α ($\times 10^{-6}$/°C at 20°C)
Water [1]	69.0
Muscovite[2]	10.6
Kaolinite[2]	11.9
Halloysite[2]	8.0
Quartz[3]	12.0
Calcite[3]	5.0
Marble[3]	5.5

[1] Lide 2010
[2] McKinstry 1965
[3] Lamond and Pielert 2006

The difference in thermal volumetric expansion between the water and soil solids leads to an excess pore water pressure in the soil. This excess pore water pressure dissipates with time, as a function of the soils permeability, the lower the permeability of the soil, the longer the time required for the dissipation of excess pore water pressure. This drainage results in a time-dependent volumetric contraction of the soil resembling the primary consolidation behavior observed during a change in effective stress (Campanella and Mitchell 1968).

The second mechanism described by Campanella and Mitchell (1968) is the decrease in shearing strength of individual particle contacts due to heating. This results in a collapsing of the soil structure and a decrease in void ratio until a soil orientation with a sufficient number of

particles is established to carry stress at high temperatures. This process continues until new bonds are developed that can handle the thermally induced stresses. This is analogous to secondary consolidation behavior under a stress increase as seen in conventional compression curves during stages of loading and reloading. Unlike the excess pore water pressure generation, this process is not considered to be reversible since no structural changes need to be made to the inter-particle bonds in order to carry the stresses resulting from subsequent cooling cycles (Campanella and Mitchell 1968).

The third mechanism of thermally-induced volume change is described by Paaswell (1967) to correlate with the decrease in pore water viscosity during heating. The change in the viscosity of pure water with temperature is described by the expression below, where μ_w is the viscosity of water ($Pa{\cdot}s$) and T is the temperature ($°C$) (Hillel 1998):

$$\mu_w = 0.00239138 - 0.00046575 \cdot \ln(T) \qquad \text{(Eq. 2.2)}$$

The viscosity of water as a function of temperature is summarized in Table 2.2. The lower viscosity values are expected to result in a slight increase in volume change during heating due to less frictional losses during outflow of water from the soil. This decrease in viscosity leads to an increase in the permeability of soil and subsequently the rate at which thermal-induced volume change occurs, as described by Kozeny-Carman equation (Mitchell and Soga 2005):

$$k = K\left(\frac{\gamma_w}{\mu_w}\right) \qquad \text{(Eq. 2.3)}$$

where k is the hydraulic conductivity, K is the absolute or intrinsic permeability, and γ_w is the unit weight of water. As the pore water flows more readily through soils with a higher permeability, an additional decrease in volume may be expected during dissipation of the excess pore water pressure.

Table 2.2: Change in viscosity of pure water with temperature (Hillel 1998)

Temperature, T (°C)	Viscosity, μ_w (Pa.s x10^{-3})
0	1.787
5	1.519
10	1.307
20	1.002
30	0.798
40	0.653
50	0.547

2.2.1 Isothermal Volume Change of Saturated Soils

2.2.1.1 Effect of Temperature on the Coefficient of Consolidation

The work performed by Finn (1951) investigated the effect of temperature on the coefficient of consolidation, c_v, the coefficient of volume compressibility, m_v, and the void ratio, e. Using an oedometer modified for thermo-mechanical testing, Compression tests were performed on remolded clay at temperature range between 5 and 26.6°C. Observations were made in the study concluding that the coefficient of consolidation does not vary significantly with temperature for temperature range of 21 to 26.6°C, but varies considerably with temperatures in the range of 5 to 21°C. Furthermore, McGinley (1983) conducted a isothermal (temperature remaining constant) compression test using an oedometer at temperature levels between 26.7 and 85°C on two types of remolded clay (Georgia Kaolin, PI = 19%, and Smectite, PI = 89%). For the two clay minerals tested, it was observed that the coefficient of consolidation is affected by the temperature level at the time of consolidation. At equal initial void ratios, higher values of c_v corresponded with higher temperature levels of each clay specimen during compression.

2.2.1.2 Effect of Temperature on Compressibility

Finn (1951) also observed that temperature had negligible effects on the coefficient of compressibility and the coefficient of recompression. Similar observations to the study by Finn (1951) were made by Campanella and Mitchell (1968) for a temperature range between 24.7 and 51.4 °C. Campanella and Mitchell (1968) carried out isothermal consolidation tests using a modified triaxial cell. Observations were made at various temperature levels on saturated Illite clay specimens, which indicate that the slope of the compressibility curves was independent of temperature as shown in Figure 2.1. Many researchers have subsequently confirmed this behavior (Plum and Esrig 1969, Tidfors and Sällfors 1989, Cekerevac and Laloui 2004).

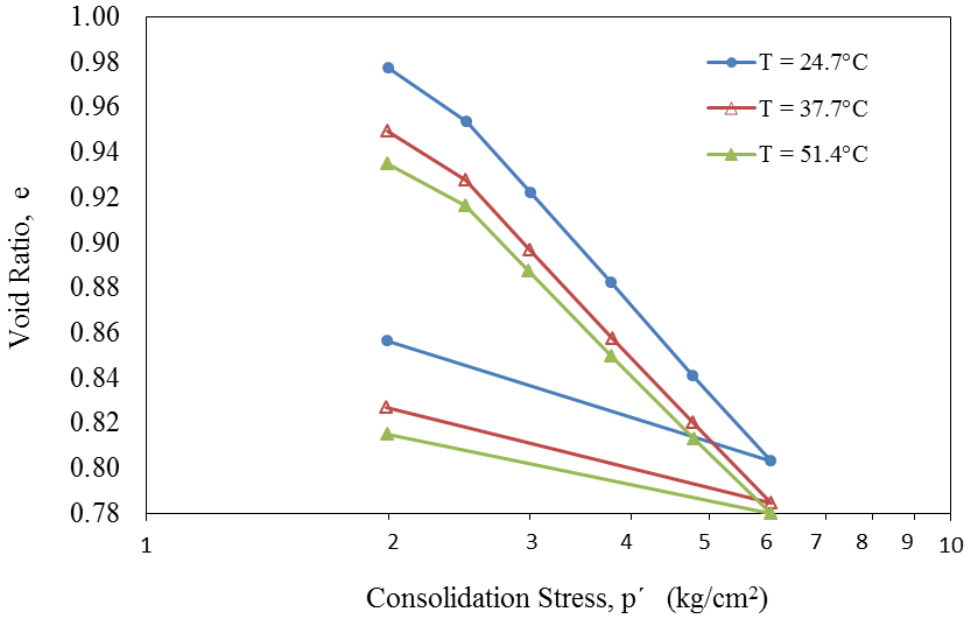

Fig. 2.1: Effect of temperature on the isotropic compression curves for saturated Illite clay (Campanella and Mitchell 1968)

Adding to the study of thermo-mechanical behavior of soils, a later study by Sultan et al. (2002) conducted compression tests on Boom clay using a isotropic compression cell. The results were not in agreement with the consolidation behavior noted by Campanella and Mitchell (1968), which shows no temperature dependence of the compressibility indexes. The results of

Sultan et al. (2002) shown in Figure 2.2, indicate that the compression curves of four samples heated to 100°C and cooled down to different temperatures converged toward the same limit. However, this study conducted isothermal consolidation tests at under higher stresses (greater than 1 MPa). It can be concluded from the observations of Sultan et al. (2002) that the thermal cycle of heating and cooling slightly decreases the compressibility at high levels of applied stress and that this effect likely depends on the soil type that is tested.

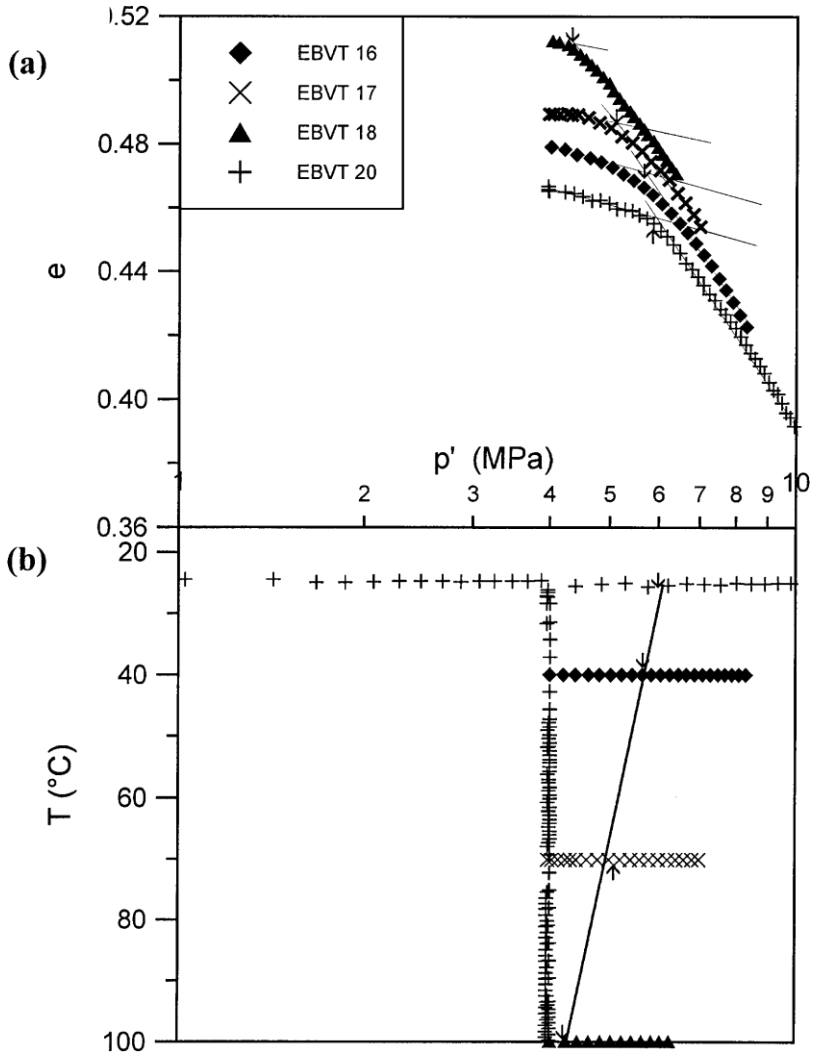

Figure 2.2: Temperature effects on compressibility at high levels of applied stress of Boom clay (Sultan et al. 2002): (a) Compression curves; (b) Temperature-stress paths

2.3 Effect of Stress History on the Thermal Volumetric Strain

Review of the literature data shows that the overconsolidation ratio has an effect on the thermal volumetric strains of a soil specimen heated under a constant stress. Dependent on the applied temperature range, soils with larger overconsolidation ratio (OCR) values tend to expand during heating while soils with smaller OCR values tend to contract. Plum and Esrig (1969) performed heated triaxial consolidation tests on remolded Illite clay (PI = 84%) between temperature ranges of 24 and 50°C with different OCR values. Figure 2.3 shows the change in thermal strains with OCR values, where positive strains and negative strains indicate expansion and contraction, respectively. The results shown in Figure 2.3 indicate that thermal expansion increases with the OCR value of Illite clay.

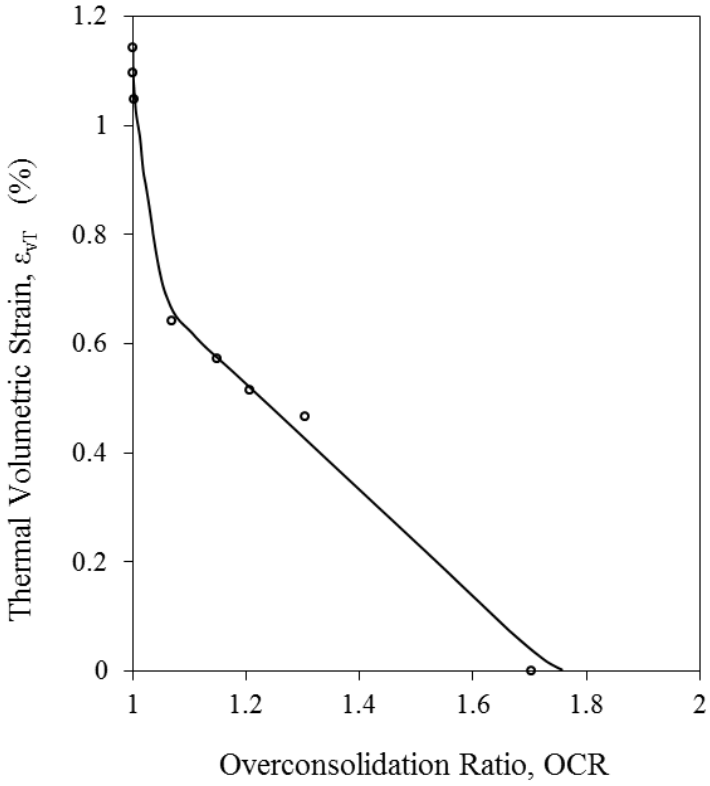

Figure 2.3: Effect of overconsolidation ratio on volume change of Illite heated from 24°C to 50°C (Plum and Esrig 1969)

Baldi et al. (1988) reported similar strain observations on remolded Pontida silty clay (PI = 12.9) tested in a high-temperature triaxial system, followed by thermal loading, and cooling. The test consisted of isothermal loading under a pressure of 2.5MPa, followed by thermal loading, and cooling. Each subsequent test was conducted identically under different stress states (OCR) and then examined for thermal volumetric strains. Strains were found to depend on the OCR and temperature of the specimen. The results seen in Figure 2.4, show that contraction was observed in specimens of low OCR (normally consolidated) and expansion was observed at high values of OCR. Other researchers have confirmed this behavior as well (Sultan et al. 2002, Cekerevac and Laloui 2004, Cui et al. 2009).

Additionally, Baldi et al. (1988) observed that the tendency of contraction increases with temperature (Figure 2.4). This temperature effect is better illustrated in Figure 2.5, which shows the volumetric strains produced when heating Kaolin clay having different OCR values. The expansion phase occurs immediately after heating until reaching a temperature of 50 °C, which is followed by expansion for clay specimens having greater OCR values. Hence, these studies show the temperature at which the thermal volume change behavior passes from an expansion to a contraction increases as OCR increases. This phenomenon was also observed by Towhata et al. (1993) and Sultan et al. (2002). The transition temperature tends to decrease nonlinearly with OCR, as shown in Figure 2.6 for the clay soil tested by Baldi et al. (1988) and Sultan et al. (2002).

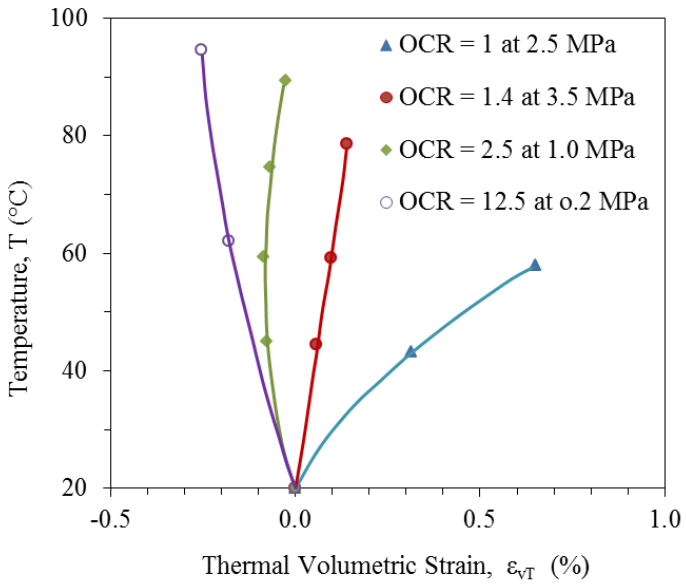

Figure 2.4: Effect of OCR and temperature on the thermal volume change of remolded Pontida clay (Baldi et al. 1988)

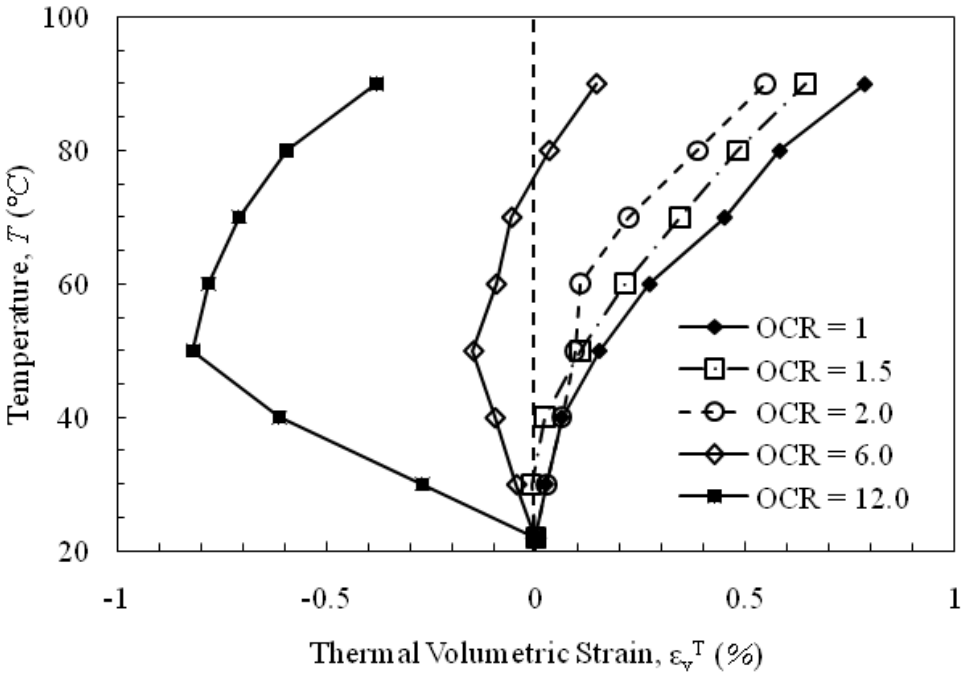

Figure 2.5: Thermal volumetric strain versus temperature during heating of Kaolin clay having different values of OCR (Cekerevac and Laloui 2004)

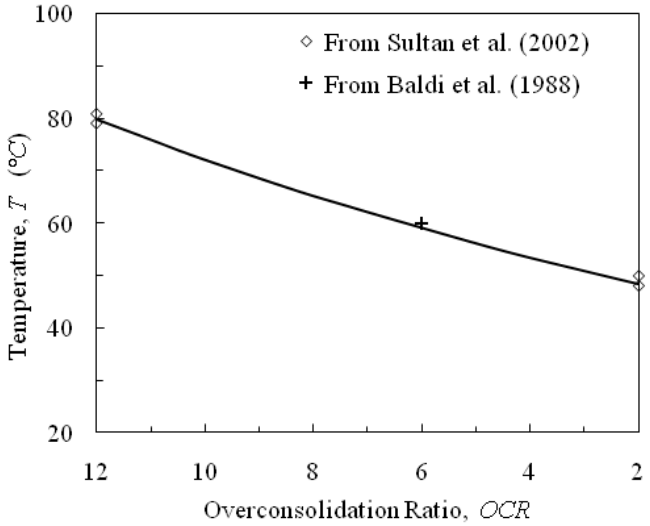

Figure 2.6: Change of expansion/contraction transition temperature with different OCRs of Pontida silty clay (Baldi et al. 1988) and Boom clay (Sultan et al. 2002)

2.4 Effects of Temperature Cycles on Thermally Induced Volume Change

Although significant efforts have been made to characterize thermally induced volume changes of soils, most studies in the past have consisted of measuring strains after a single heating and cooling. This section further describes observations occurring during temperature cycles. As previously discussed in Section 2.3, the study conducted by Campanella and Mitchell (1968) observed thermal plastic (permanent) volume reductions on normally consolidated Illite clay. During the study up to three temperature cycles of heating and cooling were imposed on the clay specimen. Figure 2.7 shows the results of the test, which conclude that plastic strains develop after the first heating cycle. It is of interest to notice that in Figure 2.7, the irrecoverable reduction in volume is large only during initial heating resembling primary consolidation. Subsequent temperature cycles produced smaller changes in volume, which decreased with further heating cycles. The minimal secondary volume change effect is observed, because the first cycle strengthens the soil because of inter-particle adjustments necessary to carry effective stresses (Campanella and Mitchell 1968). Again, this temperature-history effect is similar to the stress-history effect on volume change involving virgin compression, unloading, and reloading.

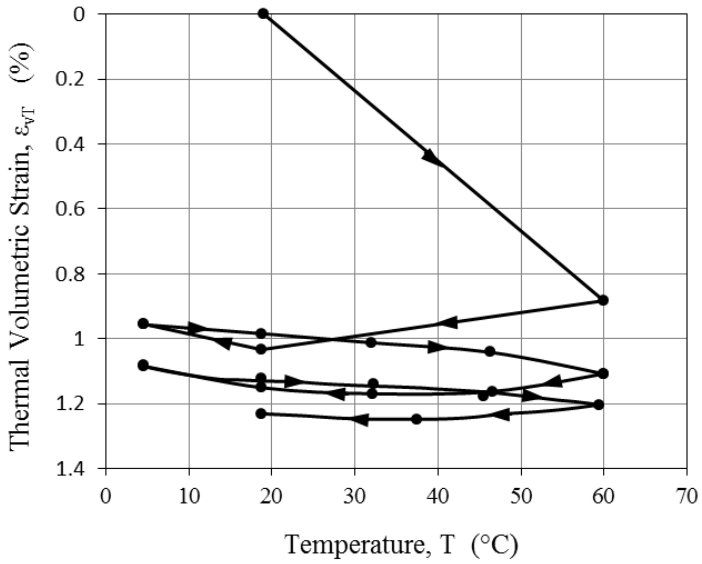

Fig. 2.7: Effect of temperature cycles on the thermal volume change behavior of saturated Illite clay (Campanella and Mitchell 1968)

As mentioned in Section 2.3, Baldi and Hueckel (1990) conducted cyclic heating and cooling test with a modified high temperature triaxial cell on Pontida clay under drained conditions. This test was performed to investigate the strain hardening effect described by previous authors. During this test, the clay specimen was subjected to the loading-temperature cycle seen in Figure 2.8. This figure describes the formation of a yield surface during the initial stage of isotropic consolidation. The clay specimen was then subjected to an increase in temperature (thermal loading) at a constant effective stress, which was followed by mechanical unloading, and the application of a second cycle of thermal loading. In agreement with Campanella and Mitchel (1968), the second loading cycle produced less volumetric strain during heating. It can be concluded that the first heating cycle induces primary consolidation, which results in plastic strain development. The strain observed on subsequent heating cycles may be due to secondary consolidation. Similar behavior during cyclic heating and cooling was also noted in the study by Burghignoli et al. (1992), who also found that the impact of a single thermal cycle had effects that depended on the overconsolidation ratio.

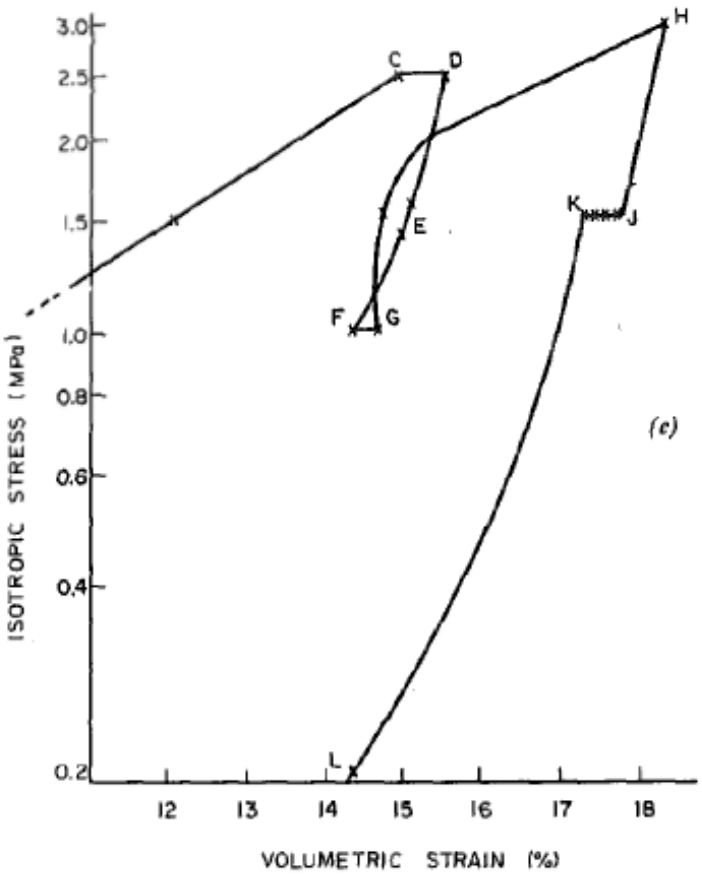

Figure 2.8: Temperature versus effective mean stress plot showing the mechanical and thermal loading cycle on Pontida clay (Huekel & Baldi 1990)

2.5 Effects of Rate of Heating on Thermally Induced Volume Change

In general, the literature shows that the thermally induced volume of soils has been well classified. However, little effort has been made to understand the impact of the rate of temperature change on the different mechanisms of thermal volume change in soils. To understand these effects, Vega et al. (2011) performed drained thermal consolidation tests on specimens of saturated Bonny silt to evaluate the impact of the rate of heating on the thermal consolidation of soil. In the study, specimens of silt were initially brought to a normally consolidated stress state in an isothermal consolidation test. Afterward, two thermal loading tests were performed by applying a fast rate of heating (55.6 °C/hr) and a slower rate of heating (10.3 °C/hr). The results of the test are seen in Figure 2.9, where each test is shown to have

similar contractive responses. This observation indicates that the total volume change at the end of a heating and cooling cycle does not depend significantly on the heating rate. Additionally, the observations from Figure 2.9 show temperature induced expansion occurring around 35 °C.

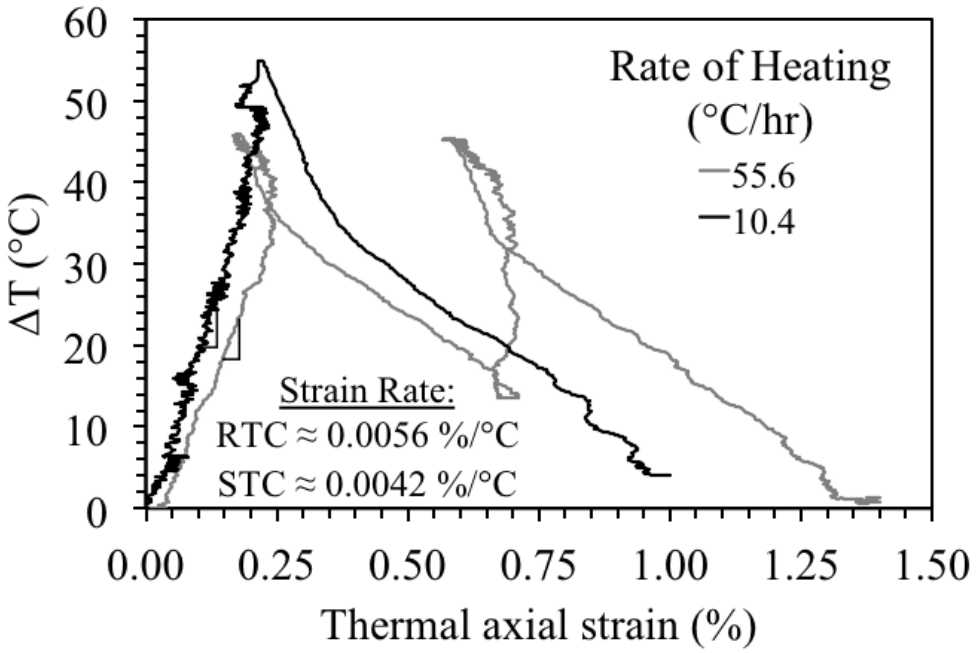

Figure 2.9: Thermal volumetric strain of NC Bonny silt for fast and slow rates of heat during thermal consolidation (Vega et al. 2011)

3. MATERIALS

3.1. Introduction

Soil from the Bonny dam located near the Colorado-Kansas border in Yuma County, Colorado, referred to as "Bonny silt", was used in this experimental study. This soil has been characterized in previous experimental studies at the University of Colorado Boulder (El Tawati 2010; Coccia 2011). Further, it is has been used in centrifuge experiments on energy foundations which involve cycles of heating and cooling (Rosenberg 2010; Stewart 2012). This chapter summarizes the various physical properties of Bonny silt, including its particle-size distribution, Atterberg limits, specific gravity, and compaction properties, compression properties, and thermal conductivity.

3.2. Particle-Size Analysis

The soil particle-size distribution of the Bonny silt was measured in accordance to ASTM D 422. The distribution of particle sizes larger than 75 μm (retained on the No. 200 sieve) was determined with a sieve analysis, while the distribution of particle sizes for the fraction that was finer than 75 μm was determined using a hydrometer analysis. The particle-size distribution curve is shown in Figure 3.1, and several particle size distribution characteristics are summarized on Table 3.1. Although Bonny silt has a high fines content, it has a wide range of particle sizes. Because of the high fines content, the silt is expected to behave as a low-permeability material which can retain stress history. Both of these features are common in soils which experience thermal consolidation (McCartney 2012).

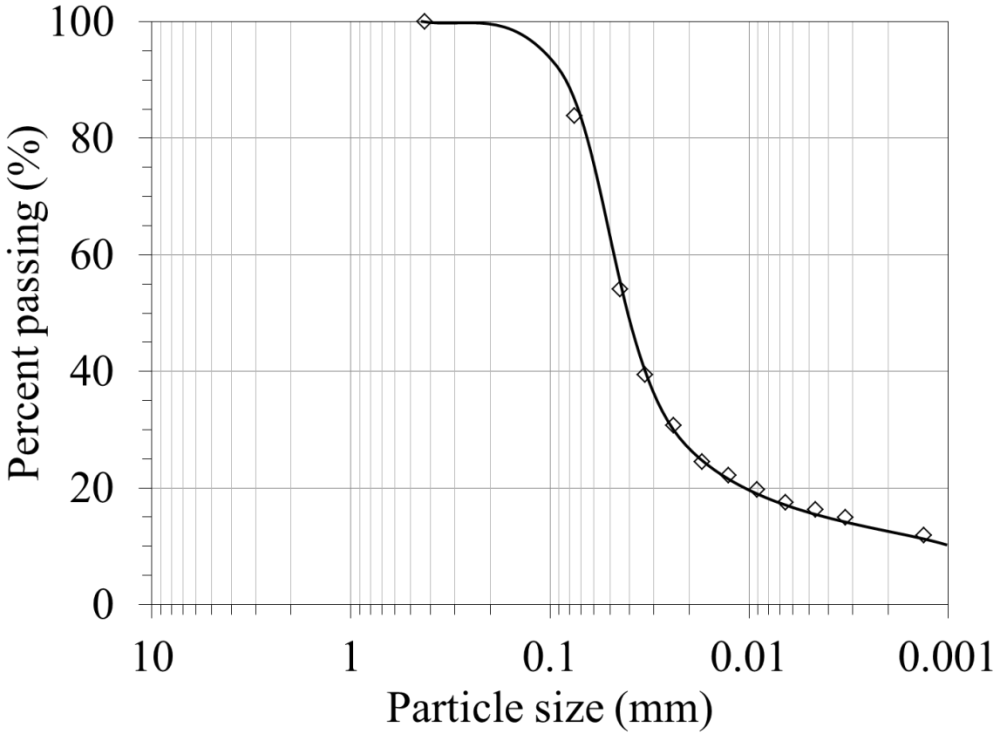

Figure 3.1: Particle-size distribution curve for Bonny silt

Table 3.1: Particle-size distribution properties of Bonny silt

Particle-Size Parameter	Value
D_{10}	< 0.0013 mm
D_{30}	0.022 mm
D_{50}	0.039 mm
% Fines (Passing No. 200 sieve)	83.9%
% Clay size	14%
% Silt size	69.9%
% Sand size	16.1%

3.3. Atterberg Limits

The Atterberg limits, which include the liquid limit (LL), plastic limit (PL), and plasticity index (PI), were measured for Bonny silt in accordance with ASTM D 4318. The results of these tests are summarized in Table 3.2, including the activity A, which is defined as:

$$A = \frac{PI}{\%\ by\ weight\ of\ claysize\ fraction} \qquad \text{(Eq. 3.1)}$$

An activity of 0.29 is relatively low, which indicates that the clay size particles do not contain a significant amount of clay minerals which have a thick diffuse double layer (Mitchell and Soga 2005). Because the thickness of the diffuse double layer of some clay minerals is sensitive to temperature, high amounts of clay minerals such as smectite may lead to complex thermo-hydro-mechanical behavior (Sultan 2002). Due to the low activity of Bonny silt, soil volume change during temperature changes is expected to occur primarily as a result of the differential thermal expansion of free water and soil particles (Mitchell and Campanella 1968). Based on the Atterberg limits and the shape of the particle size distribution, Bonny silt is classified as ML (inorganic silt) according to the Unified Soil Classification System (ASTM D 2487).

Table 3.2: Atterberg limits and activity of Bonny silt

Liquid Limit, LL	25
Plastic Limit, PL	21
Plasticity Index, PI	4
Activity, A	0.29

3.4. Specific Gravity

The specific gravity of soil solids, G_s, is defined as the ratio of the average density of particles to the density of distilled water. The specific gravity is an important parameter for calculating the weight-volume relationships for soils. The value of specific gravity for most natural soils falls within a range of 2.6 to 2.9. The specific gravity of solids that pass the 4.75-mm (No. 4) sieve (all of the Bonny silt particles) was determined by means of a water pycnometer in accordance to ASTM D 854, of the value of G_s for Bonny silt obtained as the average of three tests was 2.63.

3.5. Compaction Properties

The standard Proctor compaction test (ASTM D 698) and the modified Proctor compaction test (ASTM D1557) were performed on Bonny silt to define the relationship between compaction water content and dry unit weight for different compaction energies. The standard and modified Proctor compaction curves for Bonny silt are presented in Figure 3.2. With respect to the standard Proctor compaction test, the optimum water content, w_{opt}, for Bonny silt is 13.6% and the maximum dry unit weight, γ_{dry}, is 16.3 kN/m^3.

The specimens evaluated in this study were prepared using static compaction with a manual press in order to lead to similar soil conditions to those used in centrifuge tests on energy foundations by Rosenberg (2010) and Stewart (2012). The target compaction water content is 15% and the target dry unit weight is 16.6 kN/m^3, which is slightly wet of optimum.

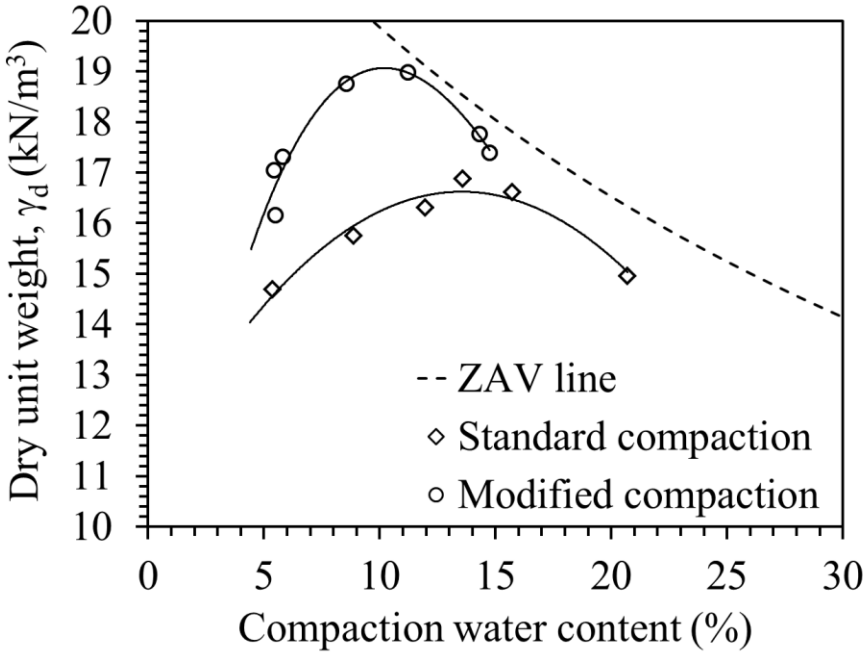

Figure 3.2: Proctor compaction curves for Bonny silt

3.6. Isothermal Volume Change Properties

The compression properties of Bonny silt were measured using a standard oedometer test (within the same cell used in the thermal consolidation tests) following the procedures in ASTM D2435, although loading increments were applied only until reaching the end of primary consolidation at each stress level. The compression curve for a specimen compacted to the target conditions described in the previous section is shown in Figure 3.3. The compression curve was corrected to account for the mechanical deflection of the apparatus, as will be described in Chapter 4. The compression curve parameters are presented in Table 3.4. A typical log-time settlement curves for Bonny silt during a stress increment of 400 kPa is shown in Figure 3.4. In general, specimen was observed to reach 90% consolidation after approximately 4.41 minutes. This corresponds to a coefficient of consolidation c_v of 1.32 cm^2/min. The value of c_v will of course vary as a function of the loading increment and void ratio.

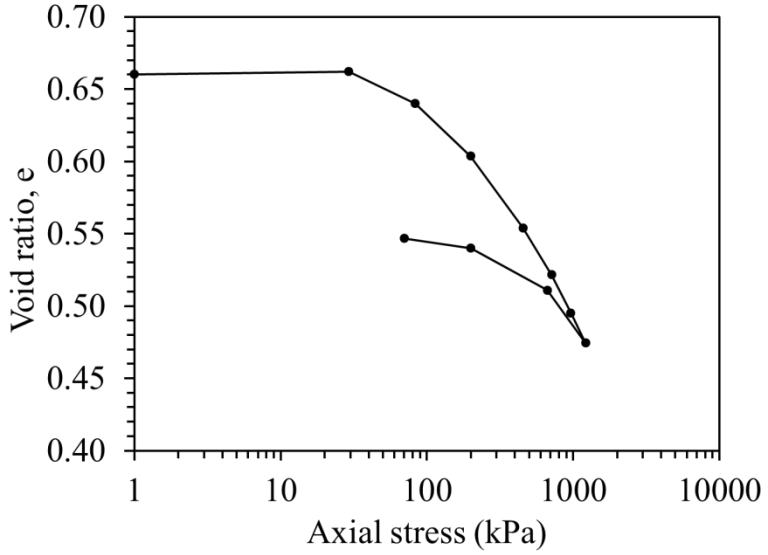

Figure 3.3: Compression curve for compacted Bonny silt

Table 3.3: Compression curve parameters

Compression Property	Value
Compression Index (C_c)	0.20
Recompression Index (C_r)	0.034

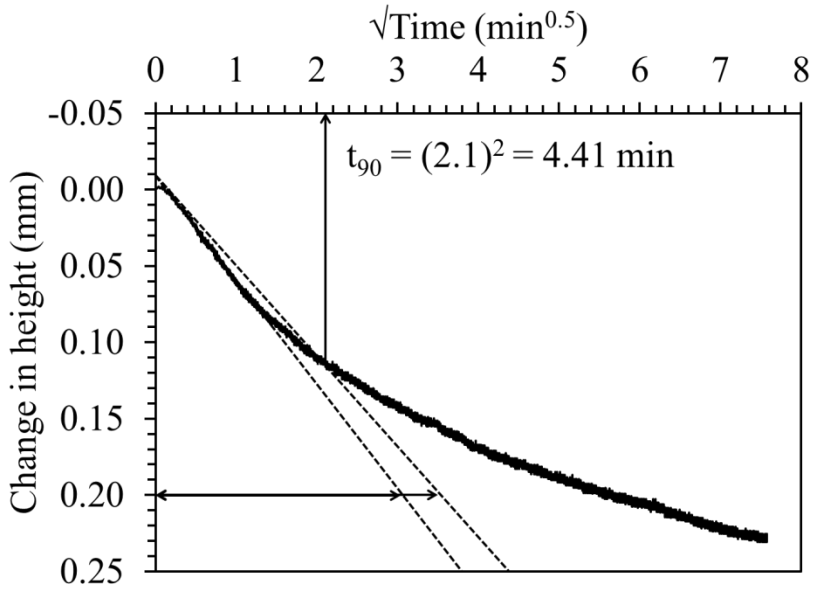

Figure 3.4: Typical time settlement curve for Bonny silt on a root-time plot

3.7. Thermal Conductivity

Thermal conductivity for Bonny silt was measured using a thermal needle test on a compacted silt specimen during isotropic compression, using the methodology described by McCartney et al. 2013). This test measures the thermal conductivity of soils as a function of void ratio using a triaxial cell modified to permit a thermal needle probe to be inserted into the soil specimen through the top platen. The thermal conductivity of Bonny silt was measured after consolidation of the specimen to different void ratios. Results from two separate tests performed on Bonny silt indicates that the thermal conductivity ranges from 1.37 to 1.47 W/(m°C) for void ratios of 0.60 to 0.52, as shown in Figure 3.4. Although isotropic compression was used in these tests, this test provides a range of thermal conductivity values for Bonny silt. Further, it should be noted that Abuel-Naga et al. (2009) found that the thermal conductivity values measured using a thermal needle test may be 30% too high using comparisons with steady-state heat flux plate tests. Accordingly, a conservative estimate of the thermal conductivity range would be 0.96 to 1.03 W/(m°C).

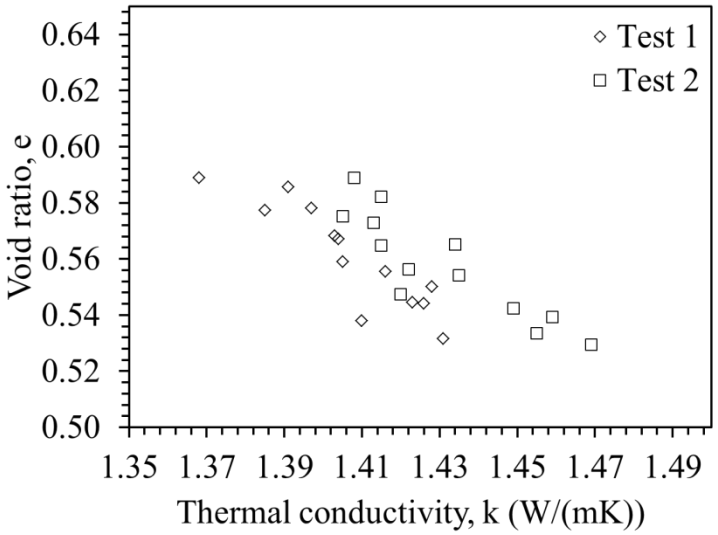

Figure 3.5: Thermal conductivity versus void ratio for Bonny silt measured during an isotropic compression test

4. EXPERIMENTAL SETUP

4.1. Introduction

A temperature-regulated oedometer developed by McGinley (1983) and modified by El Tawati (2010) was used in this study to evaluate the thermo-mechanical response of compacted silt during heating and cooling cycles. The temperature regulated oedometer system (Figure 4.1) consists of three main components: the pressure cell, the mechanical loading system, and the heating system. The system includes the following instrumentation: a load cell to measure the axial load, a linearly variable displacement transformer (LVDT) to measure axial displacement, a pressure transducer and a differential pressure transducer to measure pore water pressure changes in the soil specimen, and two thermocouples to measure the temperature of the soil specimen and water contained within the pressure cell. This chapter will discuss the main components and instrumentation of temperature-regulated oedometer system.

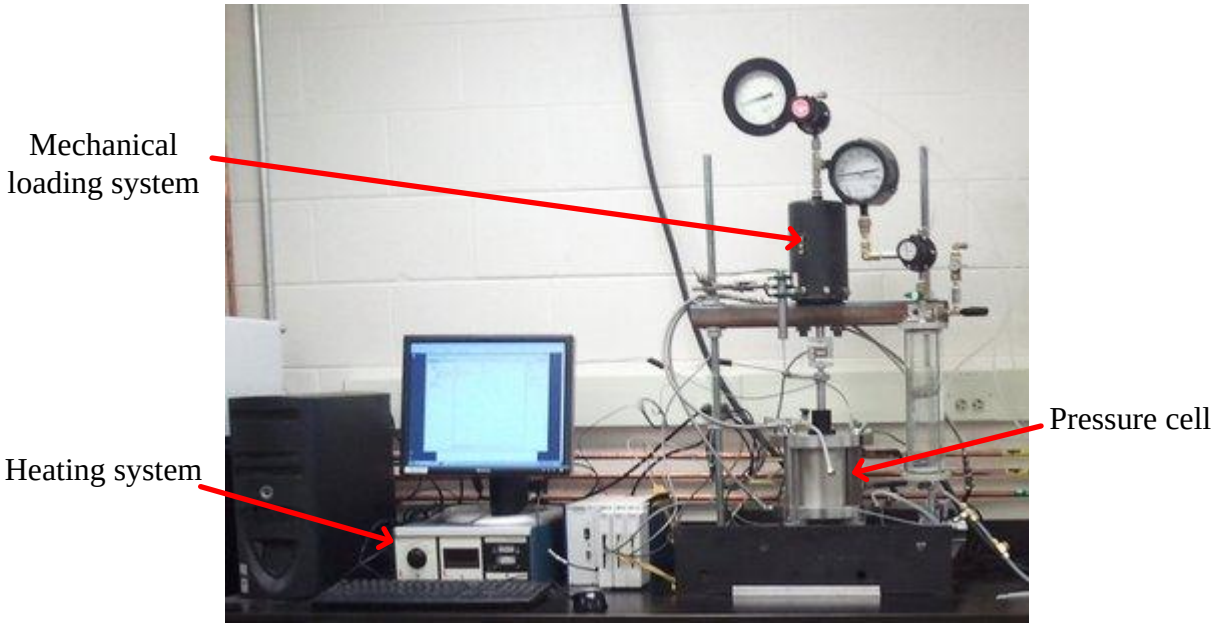

Figure 4.1: Temperature-regulated oedometer system

4.2. Pressure Cell

A schematic drawing of the pressure cell is shown in Figure 4.2. All of the main components of the cell were made of stainless steel (TYPE 316) to resist corrosion, withstand high pressures, and permit high temperature ranges. Because all of the components consist of the same metal, they will have a similar coefficient of thermal expansion, which helps minimize differential expansion and contraction of the cell components during temperature changes.

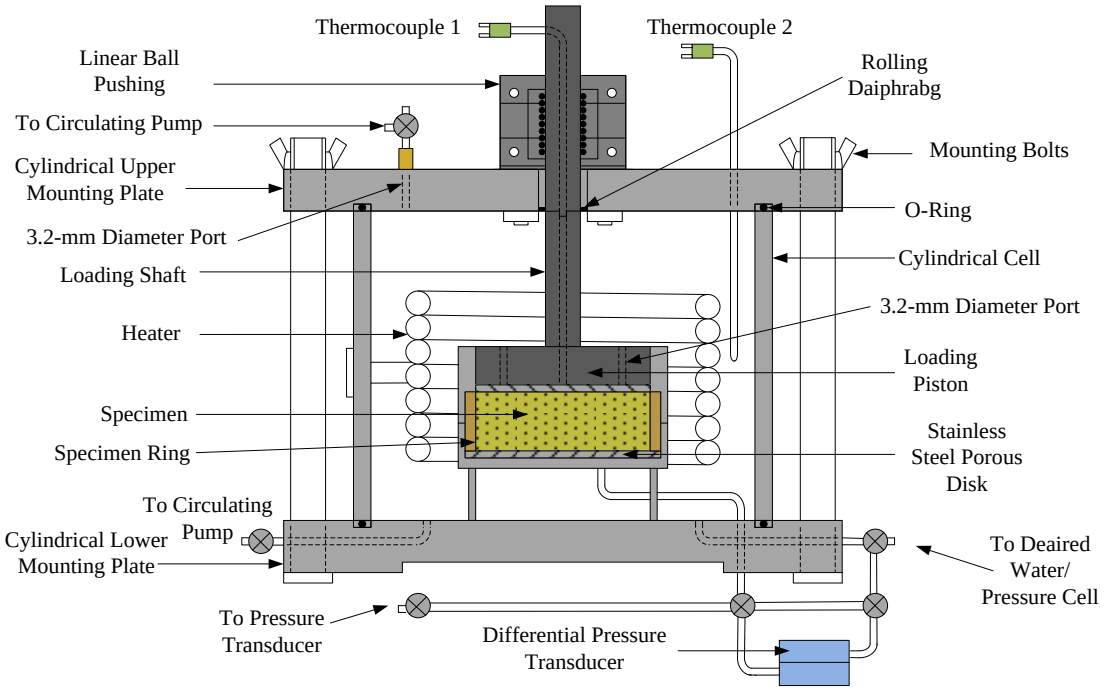

Figure 4.2: Schematic of the pressure cell

The oedometer is held within the pressure cell which has a diameter of 153 mm and a height of 127 mm. The pressure cell is formed by a cylindrical shell held between two circular plates having thicknesses of, 25.4-mm and a diameter of 83-mm, which serve as the top and bottom caps for the pressure cell. These caps have “O”-ring seals between the cylindrical shell of the pressure chamber, and are connected together using three 12.7-mm diameter bolts, as shown in Figure 4.3. El Tawati (2010) added four feet to the pressure cell to better facilitate testing and to

provide access to plumbing and instrumentation connections from the base of the cell. Heating coils are integrated into the main cylinder body of the pressure cell, which are used to heat cell water. The pressure cell includes several ports for control of the water pressure within the cell, circulation of water to homogenize temperatures, and instrumentation access. A loading piston is used to apply mechanical loads and measure displacements on the specimen. The piston passes out of the pressure cell through a linear guide bushing, and sealing is provided using a Class 4 Standard size Bellofram rolling diaphragm (cylinder bore of 22.1 mm, piston diameter of 19.1 mm, and max half stroke of 13.5 mm).

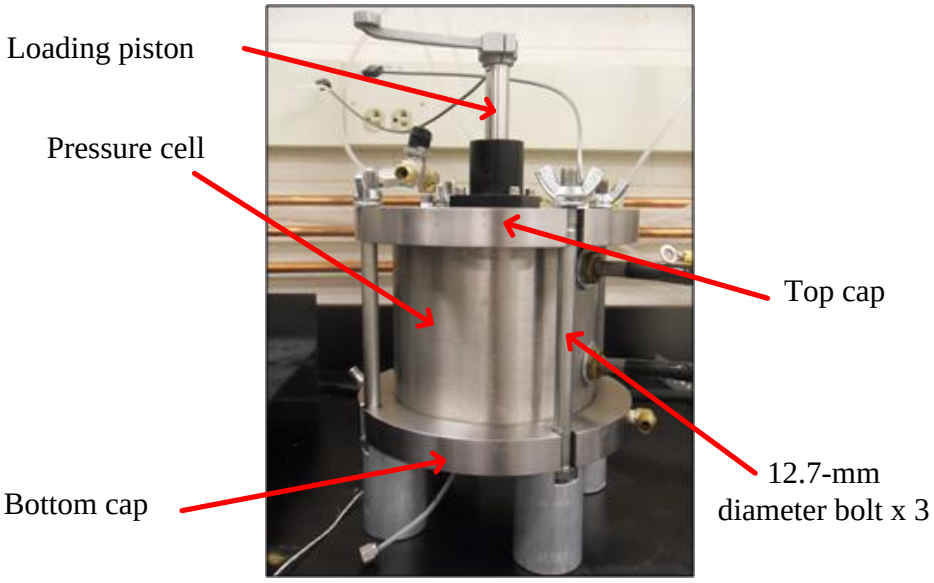

Figure 4.3: Assembled pressure cell

The soil specimen is held within a cylindrical consolidation ring which has an inner diameter of 83 mm, a height of 25.4 mm, and a wall thickness of 3.2 mm. The consolidation ring and the specimen can be removed from the system for initial compaction of the soil specimen within the ring. To help reducing friction between the consolidation ring and the travelling loading piston, the inner surface of the ring is coated with green Teflon paint. The purpose of the oedometer is to have a controlled uniaxial loading condition with free drainage at the upper boundary of the specimen and no drainage at the bottom of the specimen. This configuration allows for pore

water pressure measurements at the bottom boundary of the specimen. It is acknowledged that thermal radial expansion of the consolidation ring may not results in purely oedometric (zero lateral strain) conditions.

The bottom platen consists of a hollow steel pedestal which contains ports for a thermocouple and for a tube connected to a pore water pressure transducer outside of the pressure cell. A sintered steel porous disc is affixed to the top of the bottom platen, which permits even distribution of water pressure across the bottom of the specimen. The consolidation ring fits within a raised lip around the outside of the bottom pedestal, which is sealed using an ethylene-propylene “O”-ring. A collar having the same inside diameter as the consolidation ring is placed on top of the consolidation ring. The collar is sealed to the outside of the consolidation ring using an “O”-ring seal similar to the one used in the bottom pedestal. The collar is used to during preparation and compaction of the soil specimen, to permit swelling of the specimen above the extents of the consolidation ring, and to guide the top loading platen. The collar extends above the specimen a distance equal to the thickness of the top loading platen. The top loading platen contains a sintered steel porous disc vented to the cell through two 3.2 mm ports, which provides free drainage to the top of the specimen. The top loading platen is attached rigidly to the loading piston. Additionally, these ports allow any backpressure applied to the water in the pressure cell to be transmitted directly to the specimen. The assembled pedestal, consolidation ring, and collar are shown in Figure 4.4.

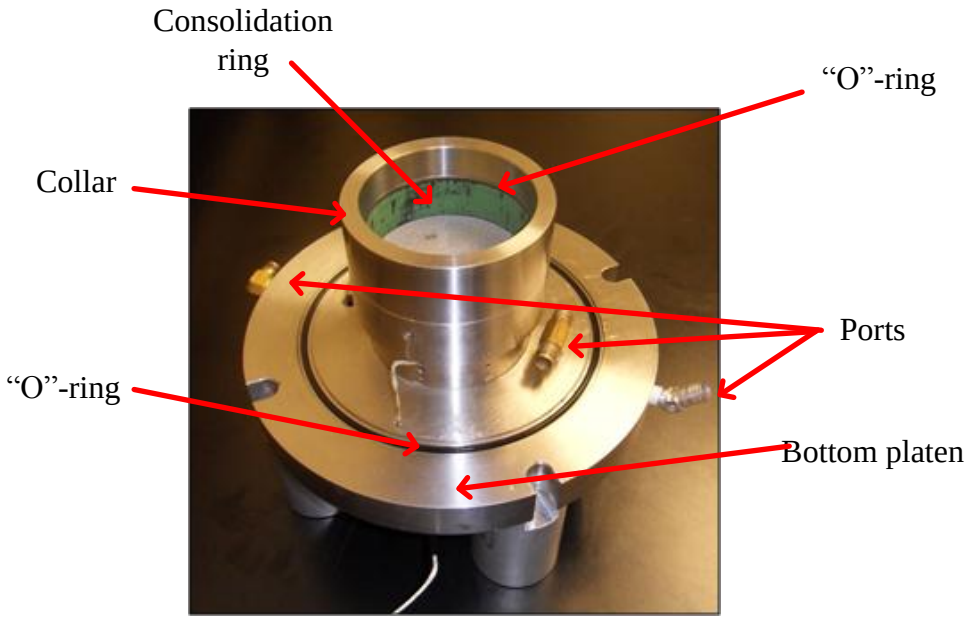

Figure 4.4: Assembled base plate, specimen ring, collar, and bottom porous disk

4.3. Mechanical Loading System.

The axial load is applied to the specimen with a loading piston that is 83-mm in diameter, which is connected rigidly to the 17.8-mm thick top loading platen. Figure 4.5 shows the top of the pressure cell and the loading piston assembly. A target for the LVDT is mounted to the top of the loading rod as shown in Fig. 4.5.

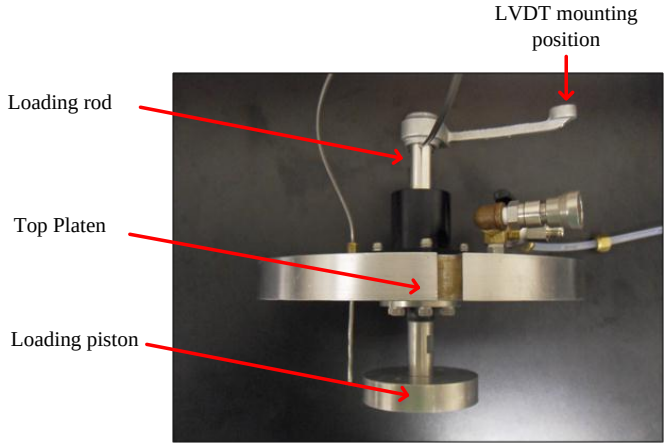

Figure 4.5: Assembled loading piston, loading rod, and linear ball bushing

A pneumatic air cylinder shown in Fig. 4.6 was used to generate the static axial load applied to the specimen. The air cylinder is a double-acting, standard diaphragm air cylinder

manufactured by Bellofram Precision Controls of Newell, WV. The cylinder has an effective area of 10323 mm^2, a stroke of 94 mm, with an operating range up to 1000 kPa. The pressure delivered to the air cylinder is controlled by a Fairchild Model 10 air pressure regulator attached to a compressed air supply having a capacity of 830 kPa. The operating range of the pressure regulator is 35 to 2070 kPa. The amount of pressure generated by the air cylinder is monitored using a Master Test pressure gauge attached to the pressure regulator. The pressure gauge is manufactured by Marsh Instruments Company and has an operating range of 0 to 690 kPa.

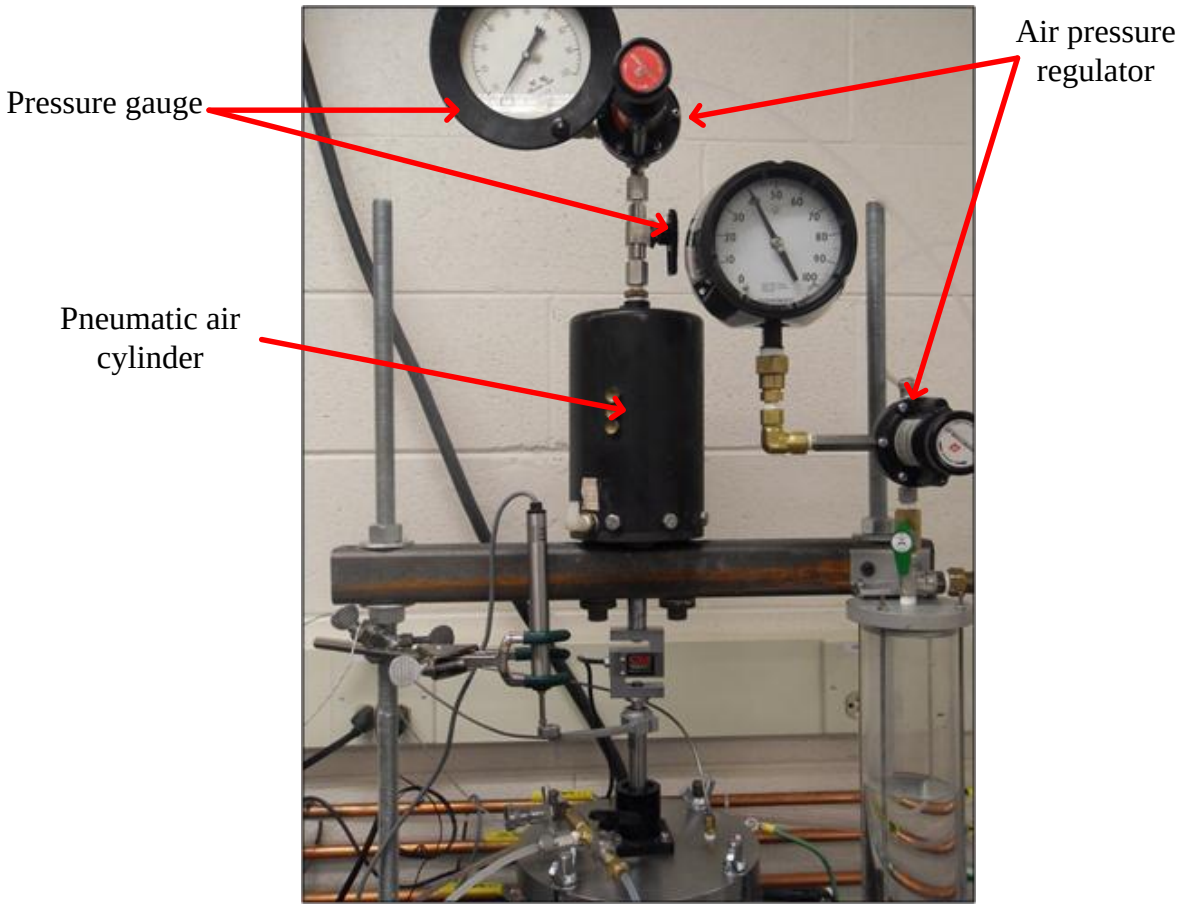

Figure 4.6: The pneumatic air cylinder, pressure regulator, and pressure gauges

A Brainard-Kilman E-210, S-type load cell, shown in Fig. 4.7, was used to measure the axial force applied to the loading piston. The load cell requires an excitation voltage of 10V DC

and operates in a load range up to 2.2 kN, with an accuracy of ±0.44 kN. The load cell is mounted to the bottom of the air cylinder rod and bears directly on the loading piston.

Figure 4.7: Load cell used to measure the axial load applied to the specimen

Axial deformations of the soil specimen during mechanical or thermal loading are measured using a linear variable deformation transformer (LVDT). The LVDT used in this study was an analog a Shaevitz Engineering Type 2002XS-D shown in Figure 4.8. The LVDT provides voltage output proportional with the displacement of the mechanical shaft. The operating linear displacement range of the LVDT is $\pm$ 50.8 mm

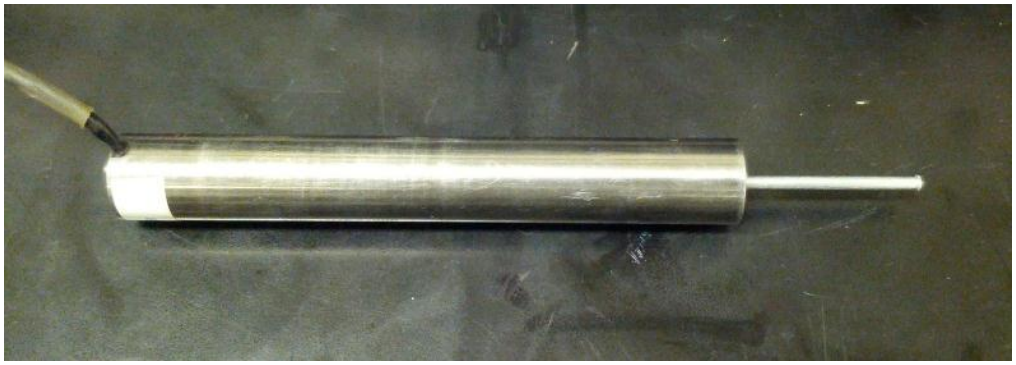

Figure 4.8: LVDT used to measure the axial deformations

4.4. Pore Water Pressure Measurement

Precise measurement of the development and dissipation of pore water pressure is an essential and crucial part of the experimental setup. Such measurement is greatly influenced by the selection of materials in the oedometer. Consequently, several precautions were taken to

ensure accurate measurements of pore water pressure. All water line connections have been constructed of stainless steel back-and-front Swagelok ferrule-type fittings to prevent possible leaks. In addition, Whitney stainless steel ball valves are used at several points in the water line system to regulate the direction of water flow. The use of stainless steel in all components enhances the accuracy of the measurement of pore water pressure because thermal expansion of the metal will cause a change in pressure within the pipes.

The backpressure applied to the water in the pressure cell is controlled using the backpressure reservoir shown in Figure 4.9. A Fairchild Model 10 air pressure regulator with an operating range of 35 to 2070 kPa is used to pressurize the water within the backpressure reservoir and the pressure cell. An in-line Ashcroft Dura-gauge pressure gauge, with an operating range of 0 to 690 kPa is utilized to measure the applied air pressure.

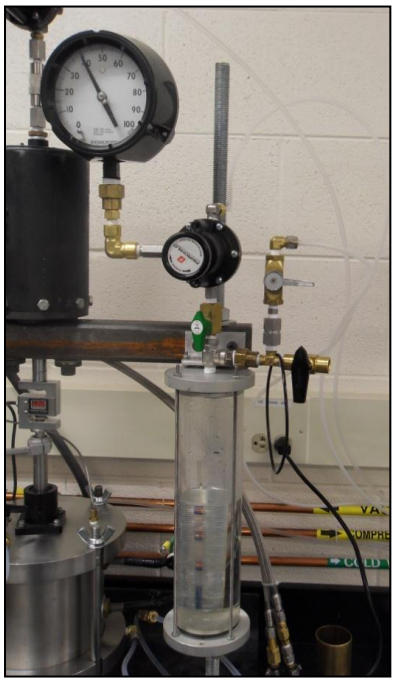

Figure 4.9: Backpressure reservoir

The water inside the backpressure reservoir was initially de-aired using a high vacuum supplied by a Precision Scientific vacuum pump (Model DD-100), shown in Fig. 4.10. The vacuum pump has a pumping speed of 4 CFM and can apply a vacuum of up to 80 kPa.

Figure 4.10: Scientific vacuum pump, Model DD-100

The absolute pore water pressure was measured at the bottom of the specimen during testing using a pore water pressure transducer (PPT), while the difference in water pressure at the top and bottom of the specimen was measured using a differential pressure transducer (DPT). The connections for the pore water pressure monitoring system are shown in the schematic in Figure 4.2. The PPT used in this study is a Brainard-Kilman E-124 model (Figure 4.11). It requires an excitation voltage of 10V DC. The PPT is enclosed in a stainless steel enclosure that has an air flushing system. The operating range for the pressure sensor is 0 to 1036 kPa.

Figure 4.11: Pore water pressure transducer

To provide a redundant measurement of the pore water pressure and to evaluate the flow processes during loading or temperature increments, a DPT was used to complement the PPT. The DPT model used in this study is a Validyne Engineering P305D model (Figure 4.12). The DPT is used to measure the difference in water pressure between the lower and upper boundaries of the specimen. It is assumed that the water pressure at the top of the specimen should remain constant during the test, equal to the backpressure applied to the cell. The DPT was connected to intercept the water line connecting to the PPT and the water line to the de-aired water reservoir.

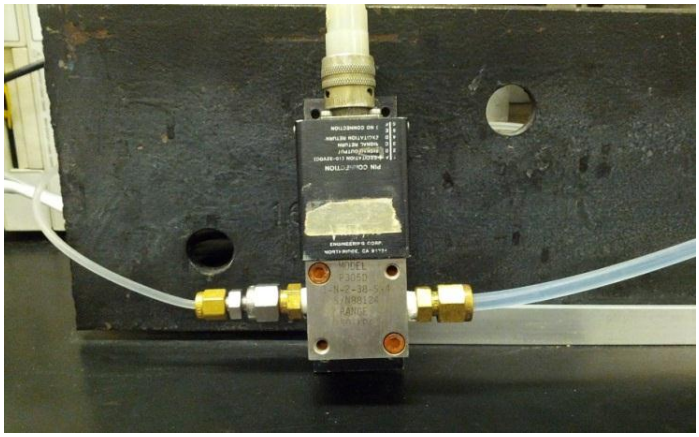

Figure 4.12: Differential pressure transducer

The load cell, pressure transducer, and LVDT were monitored using a National Instruments NI SCXI-1327, NI SCXI-1303, and NI SCXI-1315 modules respectively. These SCXI modules were mounted to a NI SCXI-1000 chassis, which is able to house, power, and control up to four SCXI modules. Collected data is transferred to the computer directly through a USB connection using an NI SCXI-1600 16-bit USB data acquisition (DAQ) and control module. The module and chassis assembly of the data acquisition system is shown in Figure 4.12

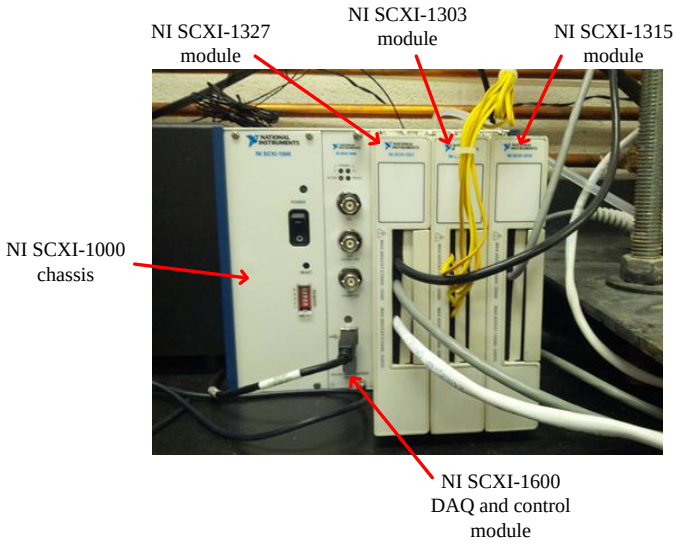

Figure 4.13: Assembled data acquisition system

4.5. Heating System

The temperature-regulated oedometer system has the capability of regulating and monitoring the temperature of testing specimen. An independently working heating system was incorporated into the device for this reason. Three essential requirements were established for the heating system:

- The heating system should work independently of the other parts of the device;
- The heating system should induce a uniform temperature field in the cell; and
- The heater should be as close as possible to the specimen in order to ensure a better temperature control.

A schematic drawing of the temperature-regulated oedometer system that includes the heating setup is shown in Fig. 4.14. The main components of the heating system are the heater, the temperature control unit, and the circulation pump.

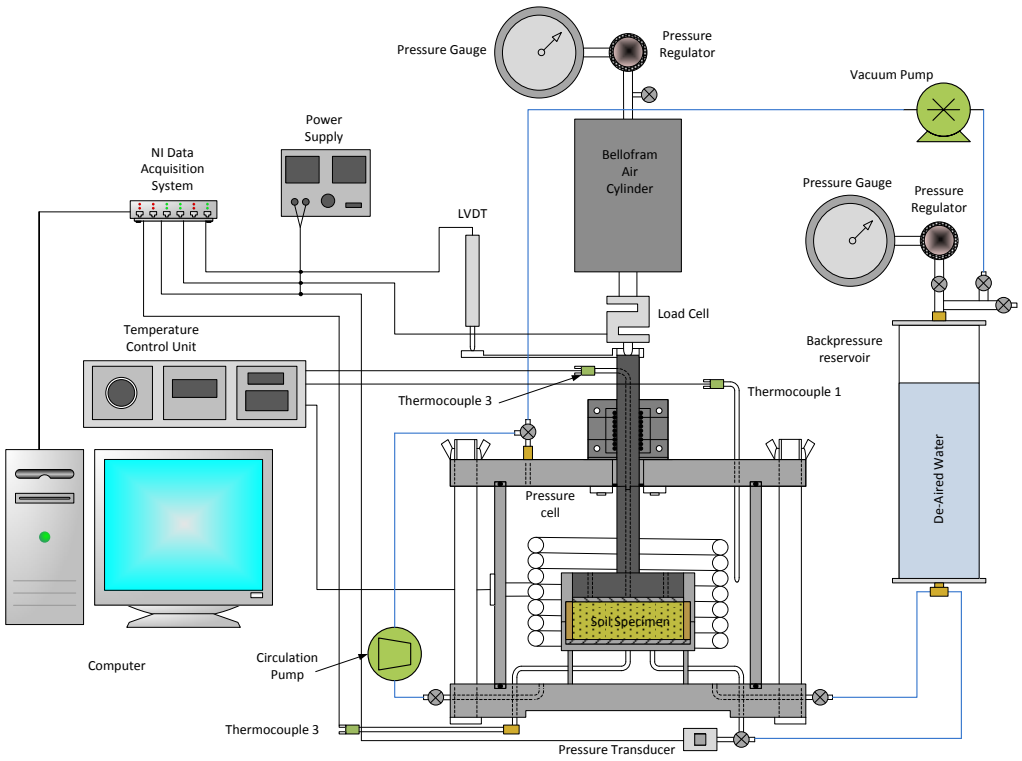

Figure 4.14: Schematic drawing of the temperature-regulated oedometer system

In order to maintain a consistent temperature of the testing environment and to obtain an efficient control of the specimen temperature, the environmental temperature was changed by regulating the temperature of the de-aired water sealed within the pressure cell. A tubular coiled heater (Figure 4.15), manufactured by Watlow Electronics with a total capacity of 4500 watt, was introduced around the sample inside the pressure cell in order to increase the temperature of the cell water. As shown in Figure 4.15, the heater completely surrounds the specimen allowing for a uniform temperature change along the circumference of the specimen. This makes monitoring of the changes in temperature of the specimen easier.

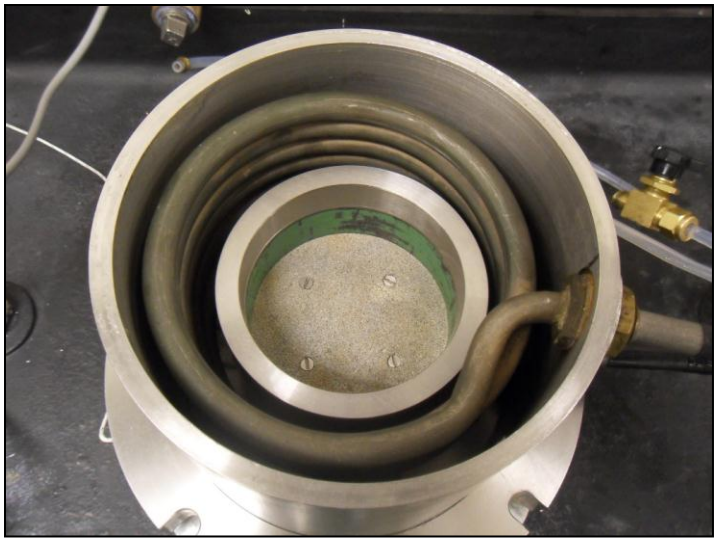

Fig. 4.15: Tubular coiled heater

Changes in temperature achieved by the coiled heater are monitored through the temperature-controlling unit, which also gives the temperature-regulated oedometer system the capability of regulating the temperature of the testing environment. Figure 4.16 shows a photograph of the temperature-controlling unit. The heater is driven and controlled by means of a manually operated electronic temperature regulator. The temperature regulator is also produced by Watlow Electronics and has an analog set control. The regulator provides an adjustable proportional band and is field selectable for an automatic on-of mode or control with an adjustable cycle time. It allows temperatures up to 205°C with an accuracy of ±1/2°C. The rate of heating produced by the temperature regulator depends on the amount of temperature increment applied; the larger the increment the higher the rate of heating. In this study, the rate of heating was the maximum rate that could be applied with the system. El Tawati (2010) used small temperature increments to apply slower rates of heating.

The environmental temperature of the temperature-regulated oedometer device is measured by 2 thermocouples and monitored in a Watlow digital temperature indicator, in conjunction with

a thermocouple switch. The digital temperature indicator, shown in Fig. 4.16, has an operating range of -190 to 870°C, with an accuracy of about ± 0.5°C.

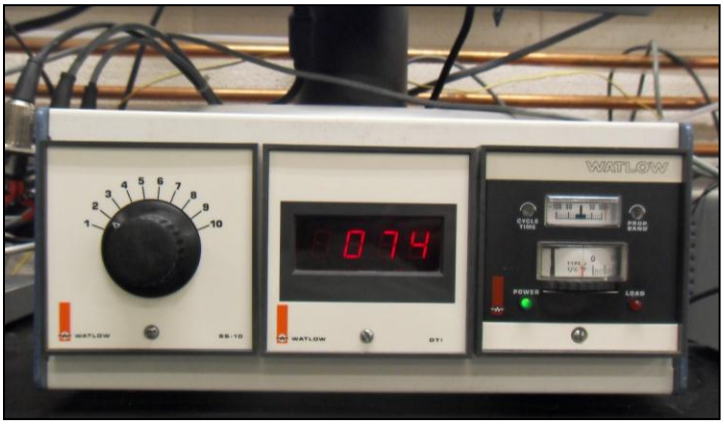

Figure 4.16: Temperature-controlling unit

To improve the temperature control of the feedback loop in the temperature control unit, a circulation pump was used to circulate the cell fluid in order to homogenize the water temperature within the pressure cell. Water was circulated utilizing an AC motor-driven gear pump (model PQM-1 from Greylor Company), shown in Figure 4.17. The pump has an operating range of temperature up to 85°C.

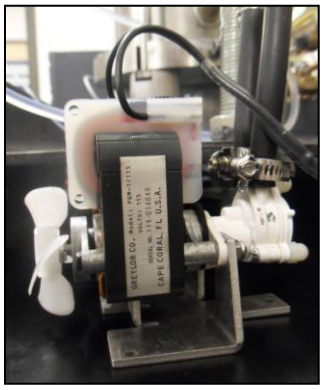

Figure 4.17: Cell fluid circulation pump

4.6. Temperature Measurement

Two tip-sensitive thermocouples were used to measure the temperature of the specimen and of the cell water. The thermocouples are stainless steel sheathed Type J thermocouples measuring 3.2-mm diameter rod. They are manufactured by Watlow Electronics and have an

operating range of -73 to 538°C, and an accuracy of $\pm$ 0.5°C. Thermocouples 1 and 2 are connected to a digital temperature indicator and data acquisition system to monitor the temperature within the cell water and at the top of the specimen. Placement of the thermocouples within the soil specimen would disturb the consolidation process. Accordingly, Thermocouple number 1 extends through the loading piston so that it can measure the temperature at the top surface of the specimen (see Figure 4.14). Thermocouple 1 was designed so that it does not extend beyond the upper porous disc. Thermocouple number 2 is situated within the pressure cell close to the coiled heater as shown in Figure 4.14 and provides a measurement of the cell fluid temperature. One of these thermocouples can be used to provide feedback to temperature controller attached to the coiled heater in order to regulate the power applied to the system to maintain a desired temperature. Thermocouple 1 was used to provide feedback to the temperature controller to regulate the temperature of the cell.

5. PROCEDURES

5.1. Setup Preparation

5.1.1. De-airing of Water in the Backpressure Reservoir

Before preparation of the specimen, the backpressure reservoir described in Section 4.4 was filled with water from an elevated water tank connected to the bottom of the backpressure reservoir. The valve at the tube line connecting the backpressure reservoir to the elevated water tank was then closed. Next, the water inside the backpressure reservoir was subjected to a vacuum of 85 kPa. The high vacuum is supplied by a vacuum pump connected to the top of backpressure reservoir (Figure 4.14). The application of a high vacuum de-airs the water inside the backpressure reservoir. This is significant in that the de-aired water of the backpressure reservoir is the supply that provides the pressure cell with water. Filling the pressure cell with de-aired water helps minimize air within the temperature-regulated oedometer system, facilitating saturation of the specimen. The water in the backpressure reservoir was placed under high vacuum for at least one hour.

5.1.2. Specimen Preparation

All soil specimens evaluated in this study were prepared in an identical manner in order to allow comparison of the compiled results to evaluate the impacts of stress state and stress history on the thermal volume change during heating and cooling cycles. The same procedure was followed in all tests for specimen compaction and placement, and all specimens were tested in saturated conditions.

The target compaction conditions were 15% gravimetric water content (wet of optimum), and 16.6 kN/m^3 dry unit weight. The soil was moisture-conditioned and stored in sealed 5-gallon bucket. To moisture condition the soil, water was added to a known weight of dry soil until

reaching the target water content and the mixture was permitted to homogenize in a closed bucket overnight. Static compaction was used to prepare the soil specimens in this study, as it was found to result in nearly identical initial soil conditions. The tools used in the compaction process are shown in Figure 5.1.

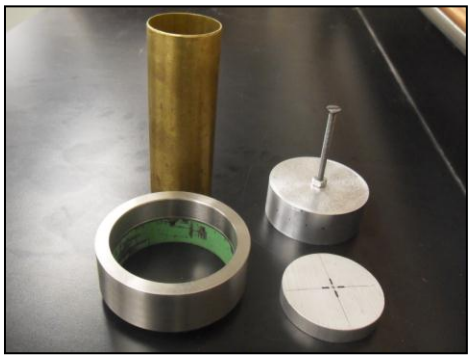

Figure 5.1: Static compaction tools

The moisture-conditioned soil was placed into the consolidation ring [Fig. 5.2(a)] in order to reach a target dry unit weight of 16.64 kN/m^3. The specimen was placed in two lifts such that the final height was slightly greater than the consolidation ring. The soil was then statically compacted inside the consolidation ring by applying a force with a mechanical press, as shown in Figure 5.2(b). The collar was placed around the consolidation ring during compaction.

(a)

(b)

Figure 5.2: Compaction of Bonny silt: (a) Placing the soil into the consolidation ring; (b) Application of static load

The soil specimen was compacted in two lifts of equal thickness to reach a uniform soil density. For each lift, the soil was compressed to a thickness of 12.7 mm under a static load of 300 kPa. The interface between the layers was scarified (Figure 5.4) to minimize the formation of a weak zone within the specimen. After compaction, the consolidation ring containing the specimen was separated from the collar. The specimen was then trimmed and weighed to calculate the actual initial unit weight. The compacted specimen contained in the consolidation ring is shown in Fig. 5.5. At least two samples were obtained for measurement of water content following ASTM D 2216.

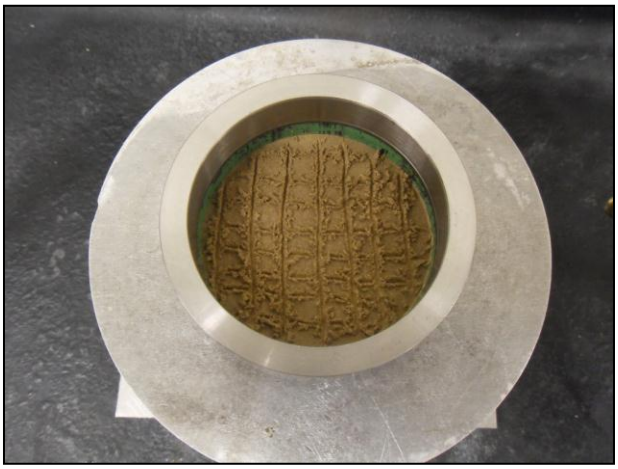

Figure 5.3: Scarified interface between the two compaction layers

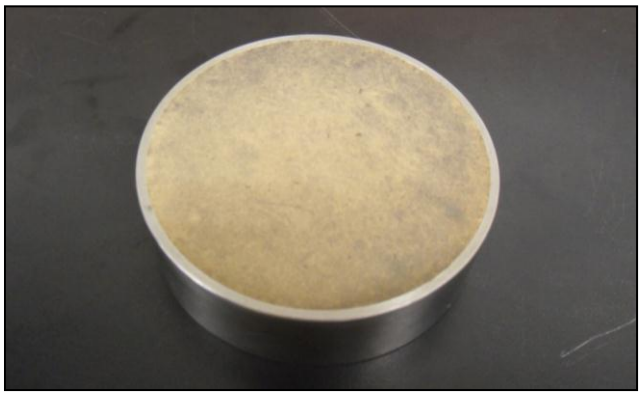

Figure 5.4: Compacted Bonny silt specimen

5.1.3. Setup of Oedometer Device

The compacted soil specimen was placed in the temperature-regulated oedometer, and the following steps were performed:

1. Filter paper was situated on top of the lower porous disk to prevent possible intrusion of the soil into the lower disk and the "O"-ring was placed around the inner surface of the raised lip (Figure 5.6).
2. The consolidation ring containing the specimen was then put in place inside the pressure cell as shown in Figure 5.7.
3. The cylindrical collar was then fitted on top of the consolidation ring and a second piece of filter paper was then placed on top of the specimen in order to prevent intrusion of soil grains into the pores of the upper porous disk (Figure 5.8).
4. The cylindrical cell, piston, sealing O-rings, and upper mounting plate were put in place, and the assembly was sealed to the base plate with four connecting bolts.

Once the pressure cell was sealed, all instrumentation were put in place and connected to the data acquisition system, and tubing and wiring were secured to the temperature-regulated oedometer system. After checking the functionality of all components, including the LabView program and instrumentation, a small seating load (equivalent to about 13.1 kPa) was applied to the specimen to prevent possible swelling of the specimen during the saturation process.

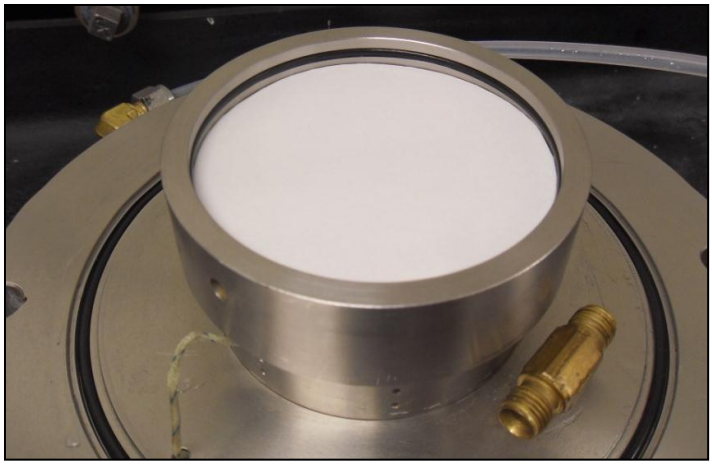

Figure 5.5: Lower filter paper and "O"-ring surrounding the consolidation ring

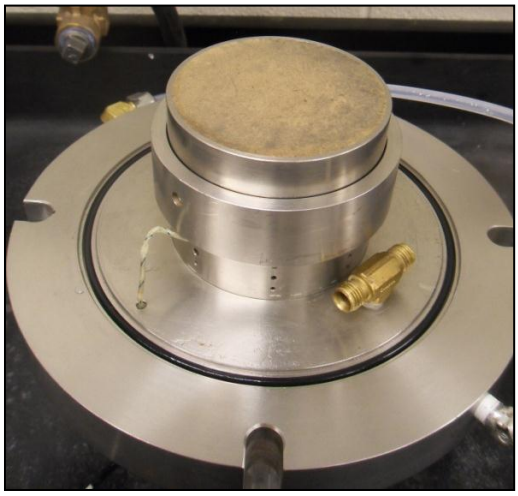

Figure 5.6: Consolidation ring containing the specimen inside the pressure cell

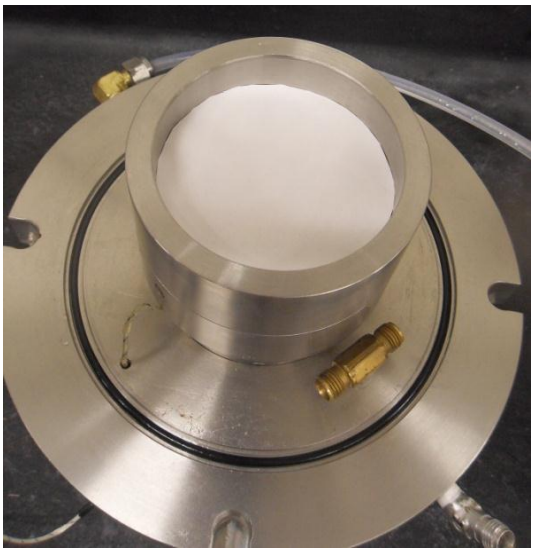

Figure 5.7: Upper filter paper atop the specimen inside the cylindrical collar

5.1.4. Soil Specimen Saturation Procedures

After application of the setting load to the specimen, a vacuum of 80 kPa was applied to the top of the pressure cell. The purpose of applying the vacuum is to replace the air inside the pressure cell and the specimen itself with vacuum to better saturate the specimen. The vacuum was allowed to act for a sufficient amount of time to ensure pulling as much air as possible out of the pressure cell as well as of the specimen. The vacuum valve from connecting the de-aired water reservoir to the bottom of the specimen was opened allowing water to saturate the specimen. This process is an efficient method of saturating the specimen as the de-aired water replaces the air voids within the specimen.

After saturation process, the vacuum valve leading to the de-aired water reservoir was closed, and the pressure cell valve was opened was opened allowing de-aired water fill the cell. To ensure that the specimen was fully saturated, the de-aired water within the pressure cell and all water lines was then subjected to a backpressure of 30 psi by applying pressurized air to the de-aired reservoir for the duration of the test. Additionally, this initial backpressure is considered as an initial value of the pore water pressure within the specimen. The valve connecting to the backpressure reservoir (de-aired water reservoir) to the lower port of the pressure cell was kept open throughout the duration of the test to permit free drainage out of the top of the specimen during application of mechanical or thermal loading.

The cell backpressure, which is the water pressure applied to the backpressure reservoir, is distributed to the top of the specimen through the ports (see figure 4.2) leading to the loading piston. This backpressure is the initial reference pressure for the specimen. Thus, any developed or dissipated pore water pressure is going to be the difference between the pore water pressure measured at the undrained bottom boundary of the specimen and the initial reference pressure.

During the application of the cell backpressure an additional axial force equivalent to the force resulted from the application of the cell backpressure on the cross sectional area of the loading rod, was simultaneously applied from the air cylinder. This axial load is required to keep the loading piston in equilibrium to avoid pushing the loading piston up outside the pressure cell.

5.2. Testing Procedures

After the assembling the temperature-regulated oedometer and saturating the specimen following the procedures described in Section 5.1.4, the mechanical and subsequent thermal tests were performed. Specifically, the specimens were loaded in an isothermal compression phase to reach a desired stress state, after which a thermal consolidation test was performed. The thermal consolidation tests were performed to evaluate the impact of temperature cycles and stress states at the same rate of heating, which was approximately from 20°C (ambient room temperature) to 90°C. A total of five tests were performed on identically prepared specimens subjected to different stress states (i.e., different overconsolidation ratios) at the end of the mechanical loading stage. The initial test, normally consolidated (NC) test, was for a specimen subjected to no unloading at the end of the isothermal compression phase, resulting in an overconsolidation ratio (OCR) equal to one. The four remaining tests were for specimens subjected to changes in stress at the end of the mechanical loading stage resulting in OCR values of 1.25, 1.67, 5.00, and 10.00. The tests are referenced according to the OCR values achieved prior to thermal loading and are as follows: NC (OCR-1), OCR-1.25, OCR-1.67, OCR-5.00, and OCR-10.00.

5.2.1. Mechanical Machine Deflections

Preliminary tests indicated that it is critical to evaluate the machine deformations during both mechanical loading and temperature changes. Accordingly, the machine deflections of the oedometer during mechanical and thermal testing were subtracted from the LVDT readings

during the isothermal compression test and the thermal consolidation test to infer the thermally induced volume changes of the specimens. The machine corrections were evaluated by placing an steel block with the same dimensions as the soil specimen within the oedometer, followed by mechanical and thermal deflection calibration tests reflecting the range of loads and temperatures used in the experimental procedures. The results for mechanical machine deflections tests are shown in Figure 5.8, where the mechanical machine deflections were calculated by subtracting the elastic deflection of the steel from the measured deflections. A positive machine deflection is defined as compression. The results indicate that the frame behaves elastically for the range of stress applied in this study.

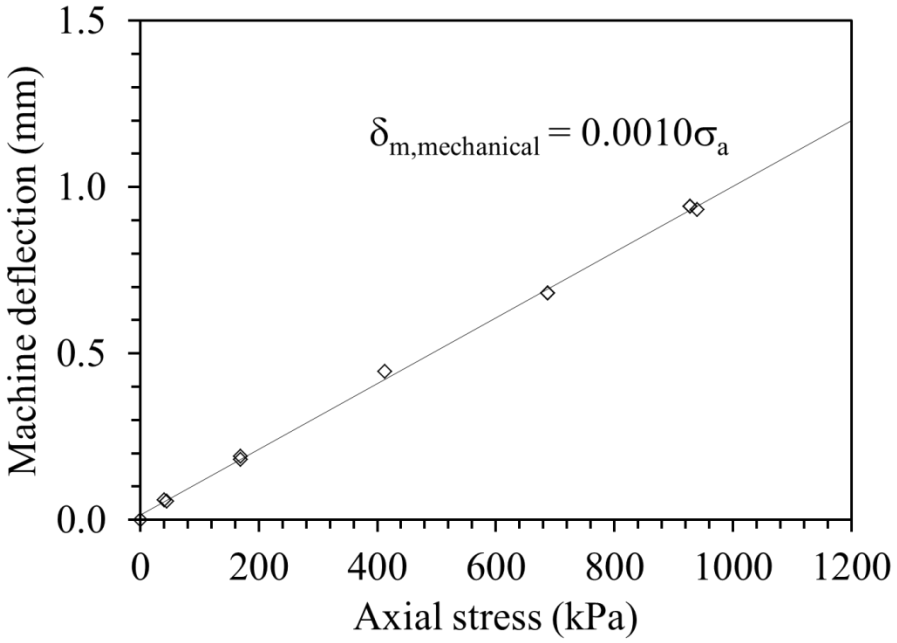

Figure 5.8: Mechanical deflections for the oedometer inferred using a steel specimen

5.2.2. Thermal Machine Deflections

The thermal deformations of the oedometer during thermal cycling were calibrated and accounted for when measuring the thermally induced volume change of the compacted silt specimens. Thermal deformations were measured using the same steel block specimen from the

mechanical deflection calibration test. The steel block was heated from the ambient room temperature approximately 90°C to evaluate the thermal expansion of the system. Machine thermal deflections were calculated by subtracting the thermo-elastic deflection of the steel block from the measured deflections. The thermal calibration test was conducted for a single heating and cooling cycle, and the time series of the temperature, theoretical steel block displacements (assuming α_{Steel} = -13×10^{-6} m/m°C), measured displacements, and calculated machine deflections are shown in Figure 5.9.

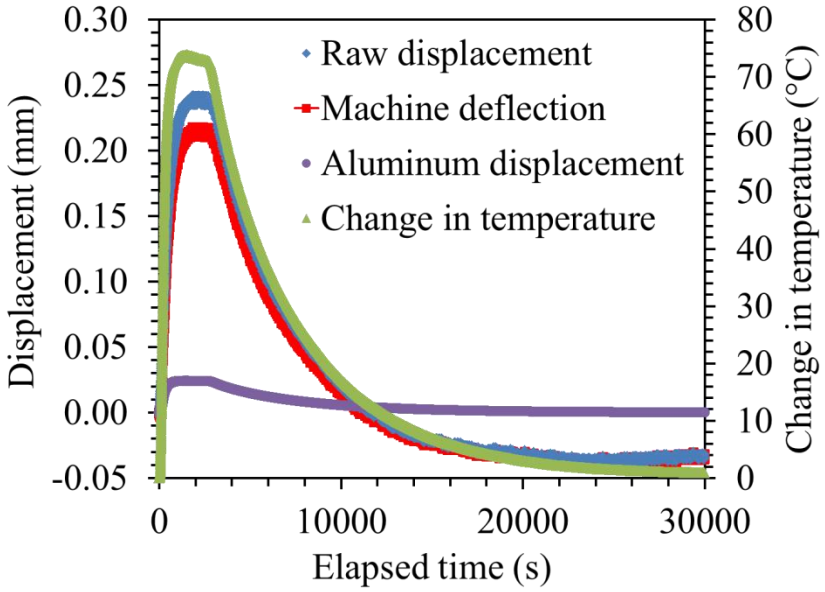

Figure 5.9: Displacement time series from the thermal machine deflection test

The machine thermal deflection of the oedometer calculated from the results in Figure 5.9 is plotted against the change in temperature in Figure 5.10. The hysteresis noted in this figure indicates that there are issues with using the steel block to infer the thermal deflections of the system. Specifically, the fact that the steel block fills the entire consolidation ring indicates that the heat flow process leads to expansion of the cell (consolidation ring) and the steel block at different rates. These thermal machine deflection curves will be improved after the defense. In the meantime, the thermal deflection data during cooling was used to correct the strains in the

soil because the deflections during cooling were nearly linear potentially because the temperature in the cell was uniform. Specifically, the slope of the cooling data was used to obtain a machine thermal deflection slope of -0.0030 mm/°C.

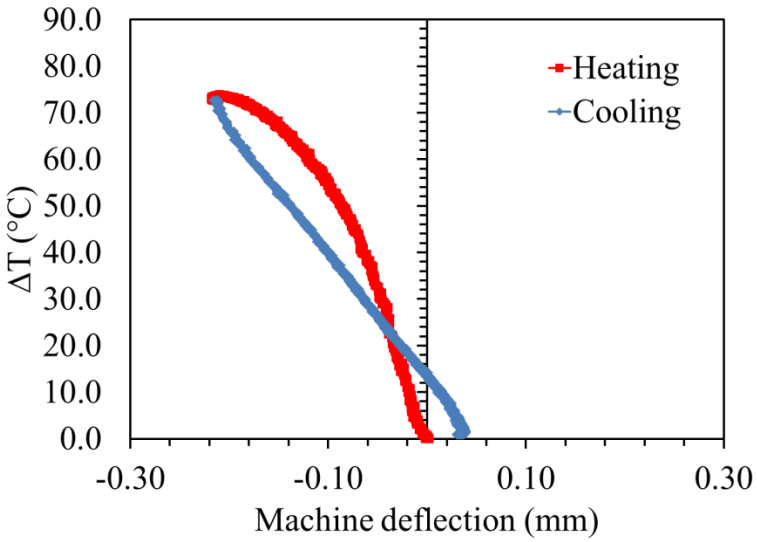

Figure 5.10: Thermal machine deflections defined using a steel cylinder

5.2.3. Isothermal Compression Phase Procedures

Each specimen was loaded to the desired stress state under ambient laboratory temperatures (~20 °C) following procedures similar to the incremental compression test procedures given in ASTM D2325. As mentioned in the literature review, the stress history of the soil, quantified by the overconsolidation ratio, has a major impact on the volume change behavior of a soil specimen heated under a constant axial stress. A schematic of the procedures followed in the isothermal compression phase for each test is shown in Figure 5.11. Following the recommendations of ASTM D2435, the highest stress applied to the specimen is intended to be equal or greater than 4 times the preconsolidation stress of the soil (which is not necessarily known because the soil was prepared using static compaction under unsaturated conditions). Each of the stress increments was maintained until the specimen reached the end of primary

consolidation. After reaching equilibration under the final stress increment, the axial load was adjusted for each test to reach the desired stress states specified by the OCR. The isothermal compression phase procedures were repeated for all five tests prior to thermal consolidation.

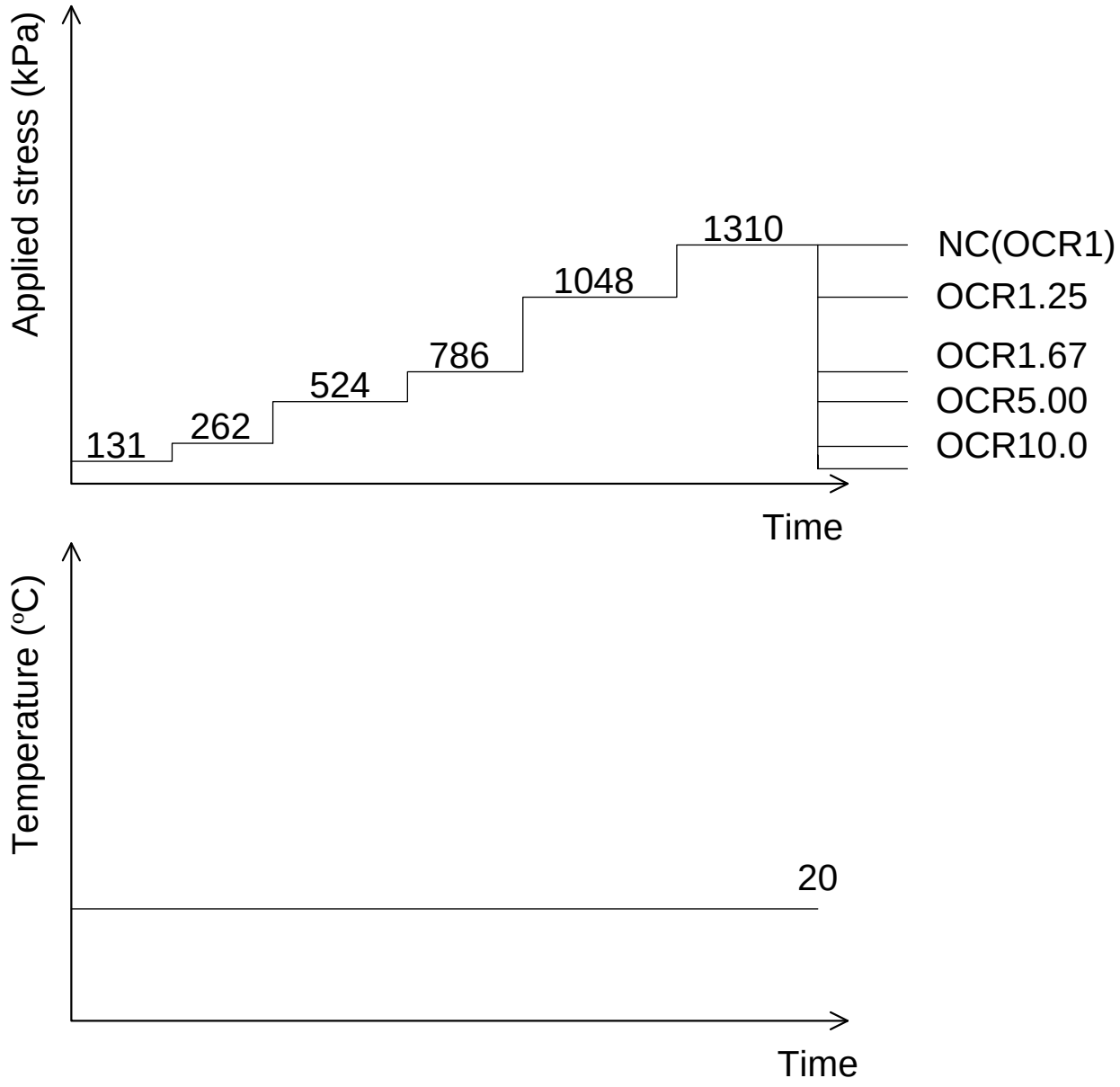

Figure 5.11: Schematic of the procedures for the isothermal compression phase

5.2.4. Thermal Consolidation Test Procedures

Five thermal consolidation tests were performed in this study on compacted Bonny silt specimens having identical preparation techniques but under different states of stress. Upon completion of the last loading increment shown in Figure 5.11, the load was adjusted in five separate tests to reach the following OCR's acting on the specimen: 1.25, 1.67, 5.00, and 10.00. Each test was then subjected to a four cycles of heating and cooling, in which the specimen was heated as fast as the temperature regulator would permit in a single stage (approximately 55.6 °C/hr) followed by unassisted cooling back to ambient temperature. The procedures of the thermal consolidation tests with specimens subjected to different stress states are shown in Figure 5.12. The goal of these thermal consolidation tests were to evaluate if the thermal strains upon re-heating were plastic or elastic and to further investigate the effect of the thermal cycle on the volume change behavior of an overconsolidated specimen. After each individual thermal consolidation test, the specimens were unloaded and removed from the temperature-regulated oedometer, weighed, oven dried, and reweighed for the determination of the final water content, w_f, and weight of soil solids, W_s.

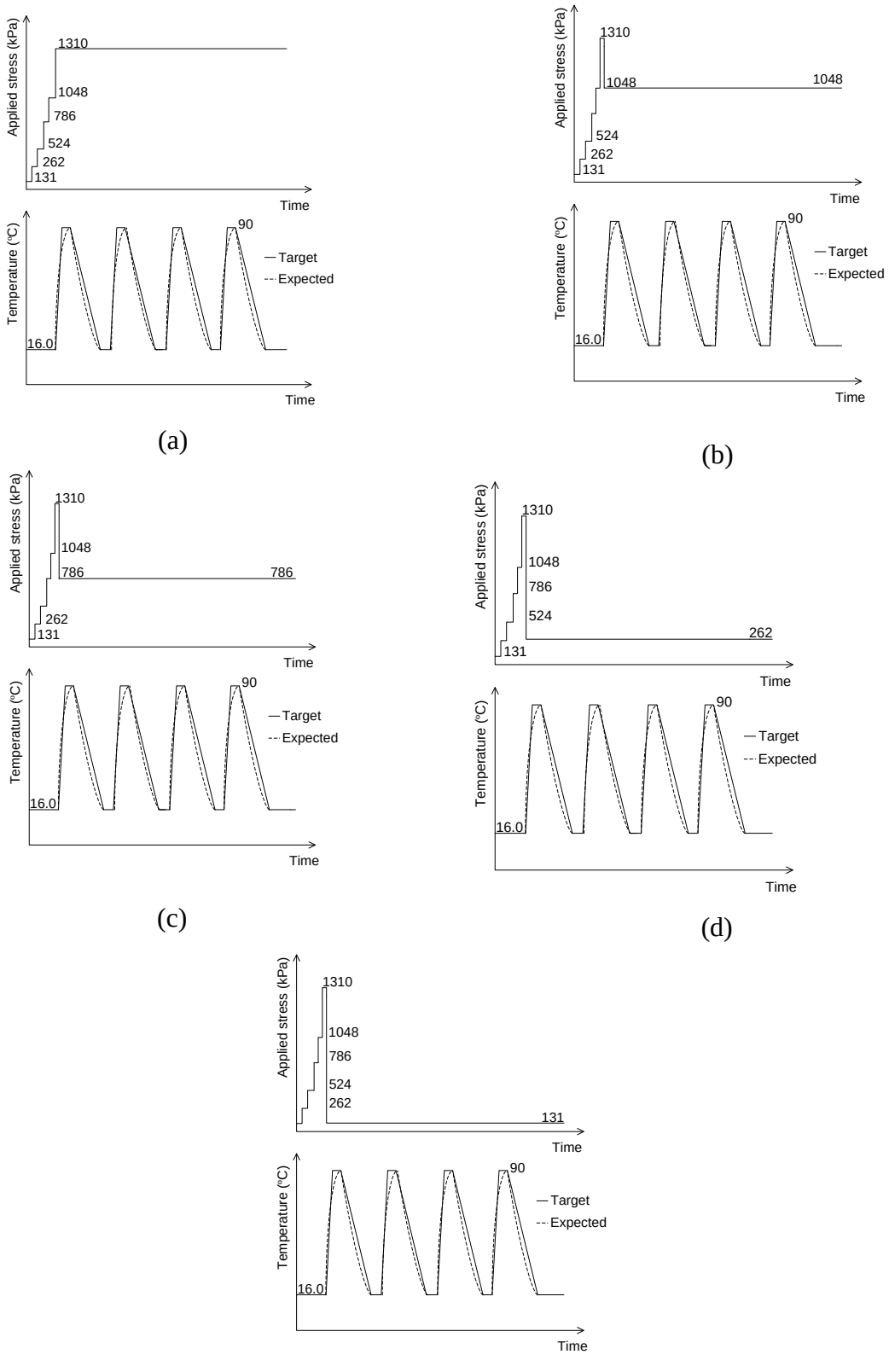

Fig. 5.12: Schematic of the procedures for the thermal consolidation tests; (a) NC-1 test; (b) OCR-1.25 test; (c) OCR-1.67 test; (d) OCR-5.00 test; (e) OCR-10.00 test

6. RESULTS

6.1. Overview

Thermal consolidation tests were performed on five compacted Bonny silt specimens consolidated to different mechanical stress states. The objective of performing these tests is to understand the impact of temperature cycles on the thermal consolidation of saturated silt under different stress states. Prior to thermal consolidation, each soil specimen was brought to a different state of stress under isothermal, room-temperature conditions (T = 20 °C). The compression curves for each soil specimen are shown for comparison in Figure 6.1. The initial compaction conditions along with the void ratio after mechanical compression are summarized for each test in Table 6.1, indicating that each specimen had similar initial conditions. Although there is some variability in the mechanical compression curves for the thermal consolidation tests performed under OCR values greater than 1, they are relatively consistent. Further evaluation of the time rate of consolidation curves for the NC test indicates that the house air pressure may have fluctuated during mechanical compression, leading to lower compression than in tests on specimens with OCR values greater than 1. Although the NC test will be repeated after the defense, the thermal response for this soil specimen provided reasonable results.

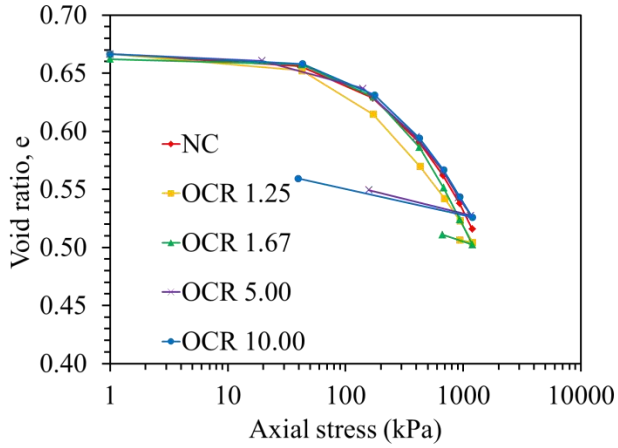

Figure 6.1: Compression curves for each of the different specimens

Table 6.1: Summary of tests and initial condition of soil specimens

Specimen number	Test name	e_i	W_i	e_c
1	NC	0.657	15.11	0.60
2	OCR 1.25	0.662	15.33	0.51
3	OCR 1.67	0.662	15.2	0.53
4	OCR 5.00	0.660	15.3	0.54
5	OCR 10.00	0.661	15.25	0.55

Note: e_i: initial void ratio after compaction
w_i: initial water content after compaction
e_c: void ratio after mechanical consolidation, prior to thermal consolidation test

6.2. Normally Consolidated (NC) Test

The goal of this test was to evaluate the changes in volume of a normally consolidated (NC) compacted silt specimen during four cycles of heating and cooling. Before thermal loading, the specimen was mechanically loaded in an isothermal consolidation test to 1310 kPa, which is exceeds the pre-consolidation stress of 400kPa, thus bringing the silt specimen to a normally consolidated stress state. Once mechanical loading was complete, the specimen was heated from the ambient room temperature to 90°C in a single rapid heating step at rate of 3.0°C/min. This first heat cycle was followed by unassisted cooling to room temperature by turning by turning off the heat source. Each subsequent temperature cycle was conducted by applying the same rates of fast heating to the silt followed by unassisted cooling to room temperature. The curve in Figure 6.2 represents the heating and cooling paths followed in the NC test. The thermal consolidation test was conducted at the end of the isothermal consolidation test under an effective stress of 1300 kPa, which was held constant. The vertical effective stress measured by the load cell throughout the test period is shown in Figure 6.3.

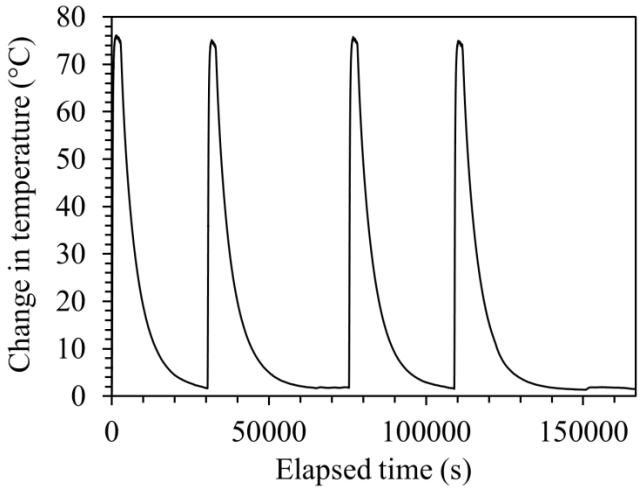

Figure 6.2: Temperature versus time for the NC test

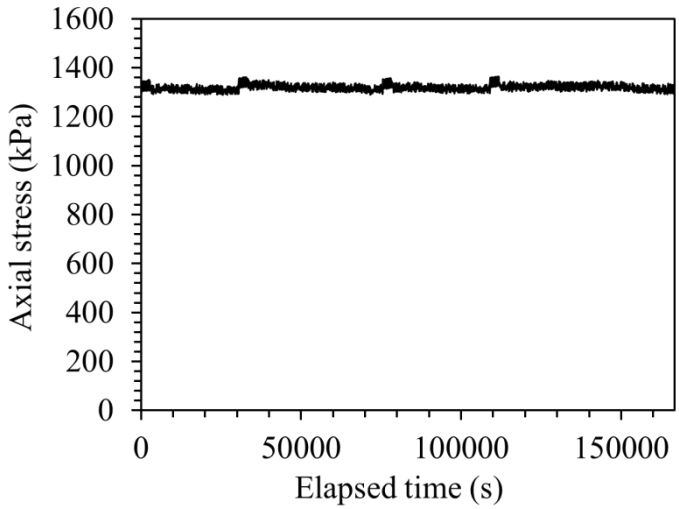

Figure 6.3: Axial stress versus time for the NC test

The excess pore water pressures generated during each heating cycle was measured using pore pressure and differential pressure transducers. Due to inconsistencies observed during testing, the changes in pore pressure measured by the DPT were used in favor of the PPT measurements. The corresponding excess pore water pressure generated during heating cycles measured by the differential pressure transducers is shown if Figure 6.4. The results of the NC test show a very rapid increase in pore water pressure corresponding with the beginning of each heat cycle, which was followed by a rapid dissipation. During each subsequent heating cycle, the

magnitude of pore water pressure generated during was observed to decrease slightly in terms of magnitude, but the absolute change was the same.

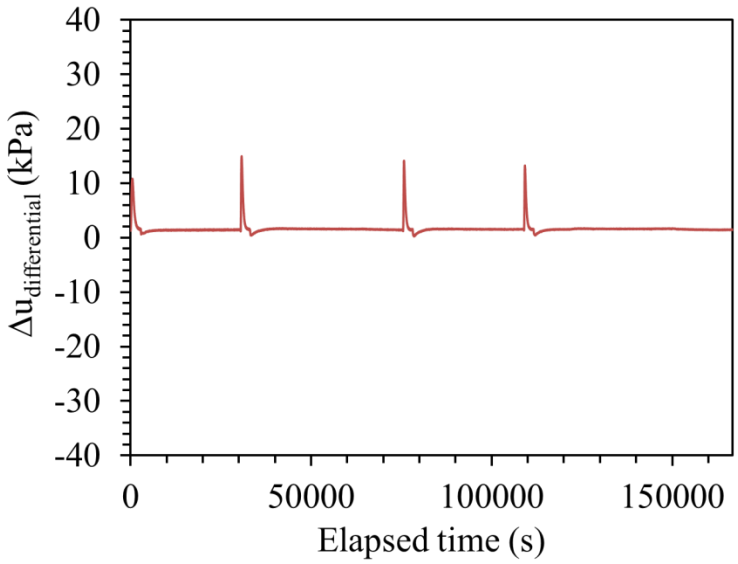

Figure 6.4: Changes in thermally induced pore water pressure measured by the DPT versus time for the NC test

During each heating cycle, the measured deflections were corrected for machine deflections that occur because of deflection of the oedometer containing the compacted silt, which occur during changes in temperature. Following the procedures detailed in section 5.2.1, the corrected deflections of the soil specimen during thermal cycling is shown in Figure 6.5(a). During each thermal cycle, the changes in excess pore water pressure correspond with the deflections of the compacted silt, as shown in the close-up in Figure 6.5(b). As excess pore water pressure is generated, the specimen was observed to contract (positive deflection), with an initially rapid rate which slowly decreased. This contraction is followed by slight expansion (negative deflection), which never fully recovers from the contraction during heating. This behavior is repeated during subsequent heating cycles, however, the magnitude of contractive deflection decreases with increasing heating cycles.

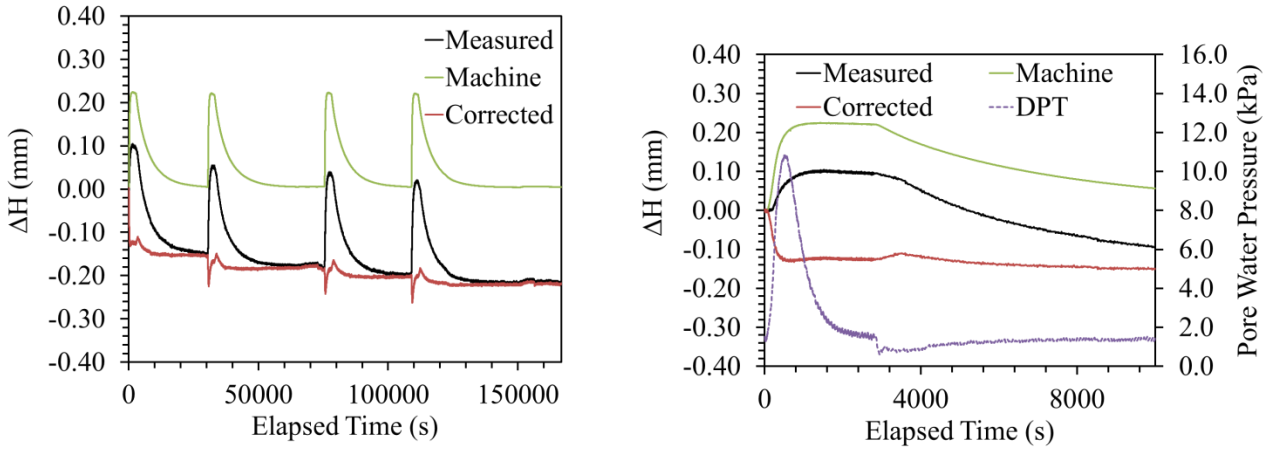

Figure 6.5: (a) Change in height versus time for the NC test; (b) Excess pore water pressure (DPT) and deflections for the NC test immediately after the first heating cycle

A summary of the results of the NC test is shown in Table 6.2. The table contains the initial and final values of the measured temperatures, rates of heating, and deflections for each temperature cycle. Further, a plot of the changes in deflection with increasing temperature cycle is presented in Figure 6.6. This figure shows that the contraction (positive deflection) of the compacted silt increases with the number of temperature cycles.

Table 6.2: Summary of results for the NC test

Temperature Cycle	Heating rate (°C/min)		Initial temperature (°C)	Final temperature (°C)		ΔH (mm)		
	Target	Measured		Target	Measured	Start of Heating	End of Heating	End of Cooling
1	1.00	1.60	16.83	90.00	91.59	0.000	-0.127	-0.155
2	1.00	1.68	18.49	90.00	90.45	-0.155	-0.163	-0.189
3	1.00	1.67	18.11	90.00	91.33	-0.188	-0.181	-0.202
4	1.00	1.65	18.55	90.00	90.77	-0.204	-0.202	-0.218

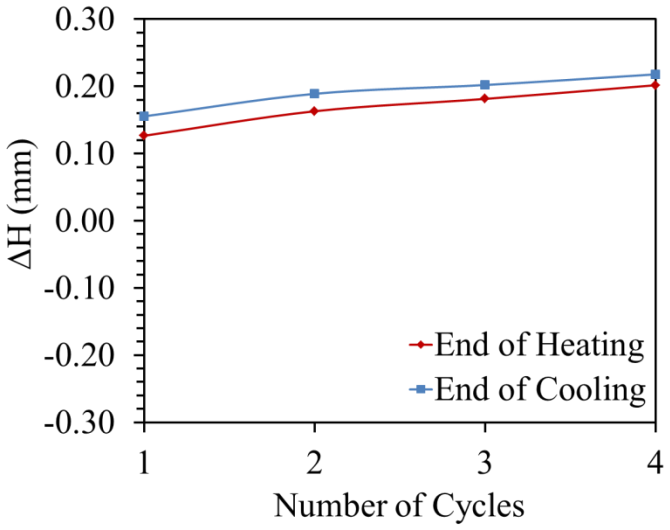

Figure 6.6: Variations in deflections with temperature cycles for the NC test

6.3. OCR 1.25 Test

This test was performed to evaluate the changes in volume of an over consolidated (OCR=1.25) compacted silt specimen during four cycles of heating and cooling. Before thermal loading, the specimen was mechanically loaded in an isothermal consolidation test to 1310 kPa and then unloaded to 1050 kPa, which resulted in an overconsolidation ratio (OCR) of 1.25. Once isothermal consolidation was complete, the specimen was heated from the ambient room temperature to 90°C in a single rapid heating step at rate of 3.0°C/min. This first heat cycle was followed by unassisted cooling to room temperature by turning by turning off the heat source. Each subsequent temperature cycle was conducted by applying the same rates of fast heating to the silt followed by unassisted cooling to room temperature. The curve in Figure 6.7 represents the heating and cooling paths followed in the OCR 1.25 test. The thermal consolidation test was conducted at the end of the isothermal consolidation test under an effective stress of 1050 kPa, which was held constant. The vertical effective stress measured by the load cell throughout the test period is shown in Figure 6.8.

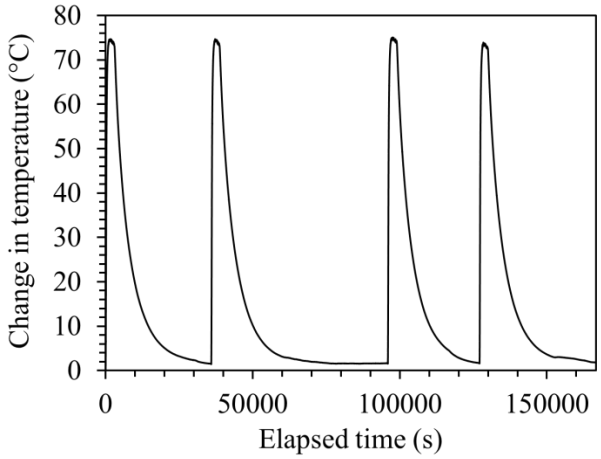

Figure 6.7: Temperature versus time for the OCR 1.25 test

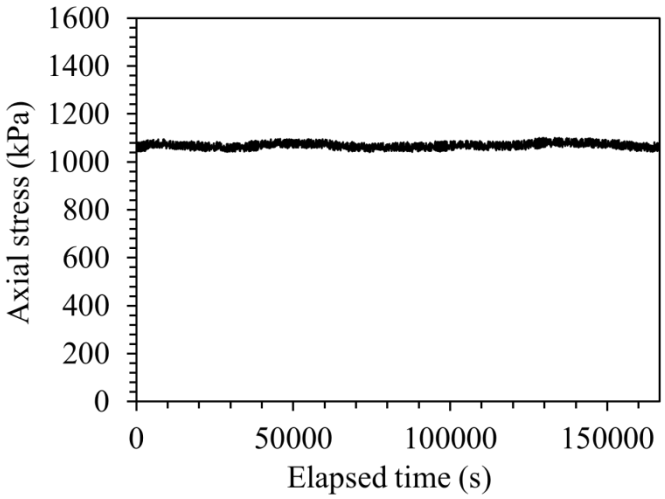

Figure 6.8: Axial stress versus time for the OCR 1.25 test

The compiled data from the test in terms of changes in excess pore water pressure and deflection and with time are presented in Figure 6.9 and Figure 6.10, respectively. In comparison to the NC test, the results of the OCR 1.25 test show a very little generation of excess pore water pressure during heating. However, a non-zero excess pore water pressure was generated at the beginning of each heat cycle, which was followed by a slow dissipation. During each thermal cycle, the changes in excess pore water pressure correspond with the deflections of the compacted silt. When observing the deflection occurring immediately after the first heating cycle

(Figure 6.10), the specimen was observed to expand slightly (negative deflection) and then contract (positive deflection) as the specimen cooled. This behavior continues for the remaining cycles, which results in a small net accumulation of contractive deflection by the end of the test.

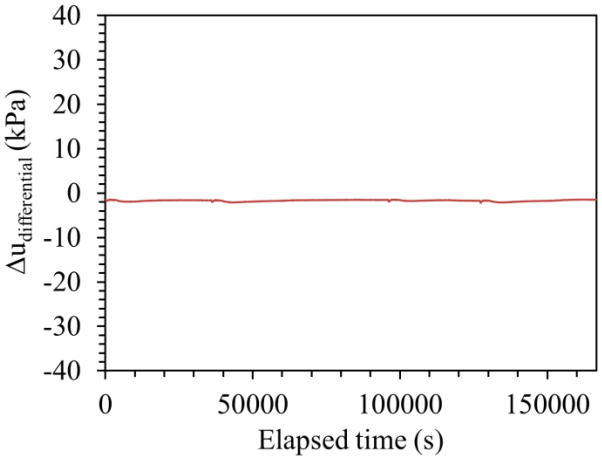

Figure 6.9: Changes in thermally induced pore water pressure measured by the DPT versus time for the 1.25 test

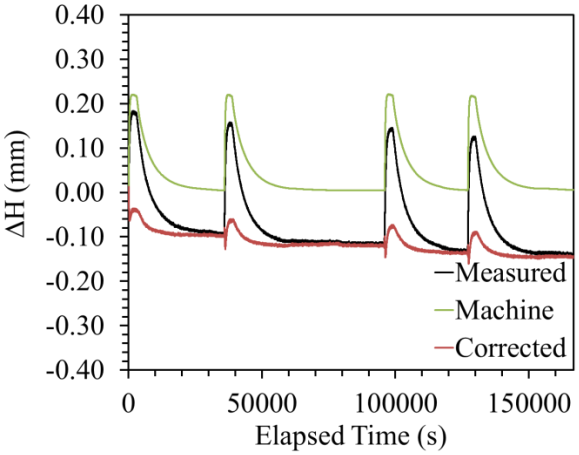

Figure 6.10: Change in height versus time for the OCR 1.25 test

A summary of the results of the OCR 1.25 test is shown in Table 6.3. The table contains the initial and final values of the measured temperatures, rates of heating, and deflections for each temperature cycle. Further, a plot of the changes in deflection with increasing temperature cycle is presented in Figure 6.11. This figure shows that the contraction (positive deflection) of the

compacted silt increases with the number of temperature cycles for the NC test. In comparison with the NC test, there appears to be slightly less contraction of the soil.

Table 6.3: Summary of results for the OCR 1.25 test

Temperature Cycle	Heating rate (°C/min)		Initial temperature (°C)	Final temperature (°C)		ΔH (mm)		
	Target	Measured		Target	Measured	Start of Heating	End of Heating	End of Cooling
1	1.00	1.47	16.70	90.00	90.02	0.000	0.041	0.097
2	1.00	1.53	18.25	90.00	90.00	0.099	0.063	0.118
3	1.00	1.43	18.35	90.00	90.74	0.120	0.078	0.136
4	1.00	1.51	18.41	90.00	89.32	0.136	0.093	0.145

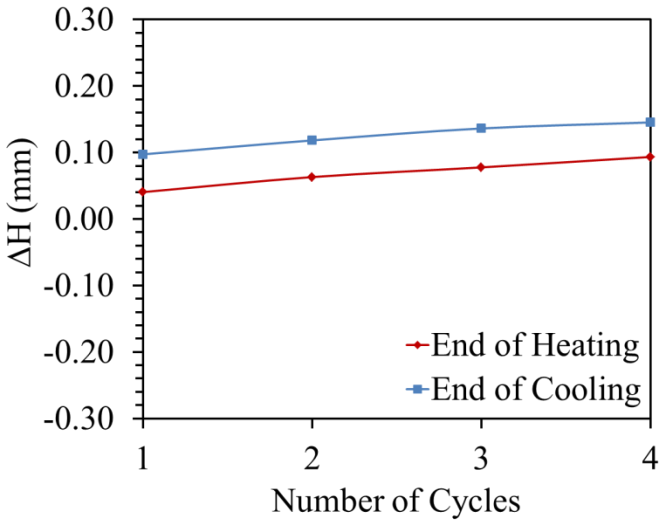

Figure 6.11: Variations in deflections with temperature cycles for the OCR 1.25 test

6.4. OCR 1.67 Test

This test was performed to evaluate the changes in volume of an over consolidated (OCR=1.67) compacted silt specimen during four cycles of heating and cooling. Before thermal loading, the specimen was mechanically loaded in an isothermal consolidation test to 1310 kPa and then unloaded to 1050 kPa, giving an overconsolidation ratio (OCR) of 1.67. Once isothermal consolidation was complete, the specimen was heated from the ambient room temperature to 90°C in a single rapid heating step at rate of 3.0°C/min. This first heat cycle was followed by unassisted cooling to room temperature by turning by turning off the heat source. Each subsequent temperature cycle was conducted by applying the same rates of fast heating to the silt followed by unassisted cooling to room temperature. The curve in Figure 6.12 represents the heating and cooling paths followed in the OCR 1.67 test. The thermal consolidation test was conducted at the end of the isothermal consolidation test under an effective stress of 1050 kPa, which was held constant. The vertical effective stress measured by the load cell throughout the test period is shown in Figure 6.13.

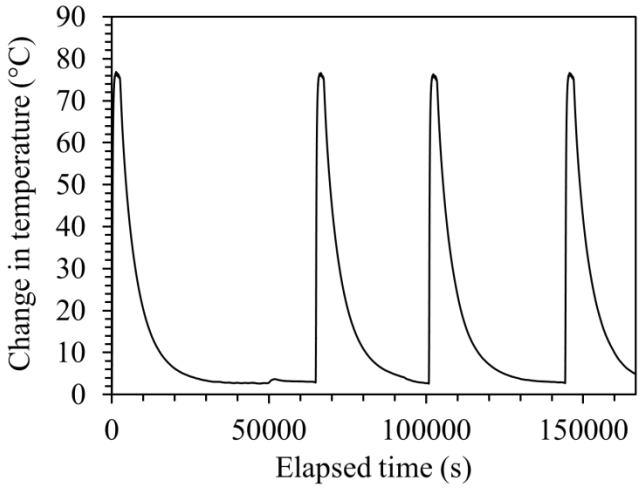

Figure 6.12: Temperature versus time for the OCR 1.67 test

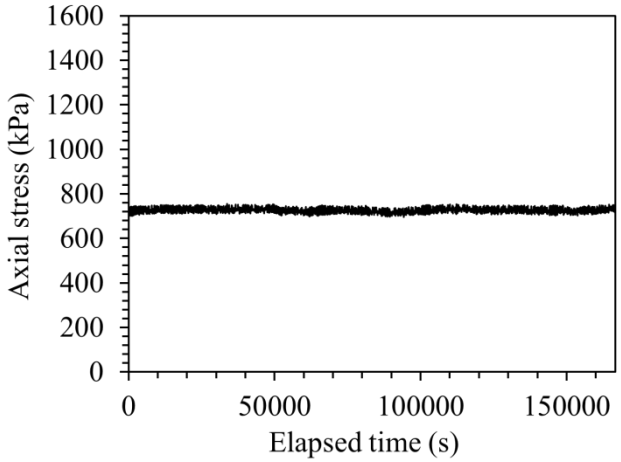

Figure 6.13: Axial stress versus time for the OCR 1.67 test

The excess pore water pressures generated during each heating cycle was measured using pore pressure and differential pressure transducers. The corresponding excess pore water pressure generated during heating cycles measured by the pore pressure and differential pressure transducers is shown if Figure 6.14. As with the OCR 1.25 test, the OCR 1.67 test showed very little excess pore water pressure was generated through each heating cycle. The general trend observed in this test is similar to the OCR 1.67 test, which had smaller magnitudes of pore water pressure with an increase in the number of heating and cooling cycles.

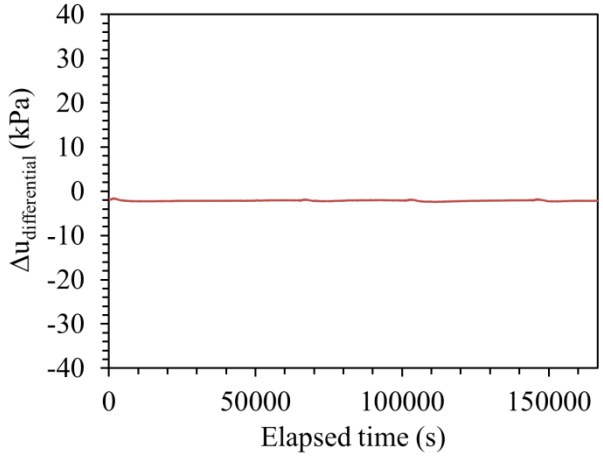

Figure 6.14: Changes in thermally induced pore water pressure measured by the DPT versus time for the OCR 1.67 test

The measured deflections that correspond with each heating cycle are observed in Figure 6.15. Similar to the OCR 1.25 test, the silt specimen expanded after the first heating cycle and contracted during cooling. However, after the initial contraction there appears to be no further accumulation of deflection at the end of the test. A summary of the results of the OCR 1.67 test is shown in Table 6.4. The table contains the initial and final values of the measured temperatures, rates of heating, and deflections for each temperature cycle. The cycle versus deflection plot in Figure 6.16 further reflects that there is almost no change in the height of the specimen after the test is completed.

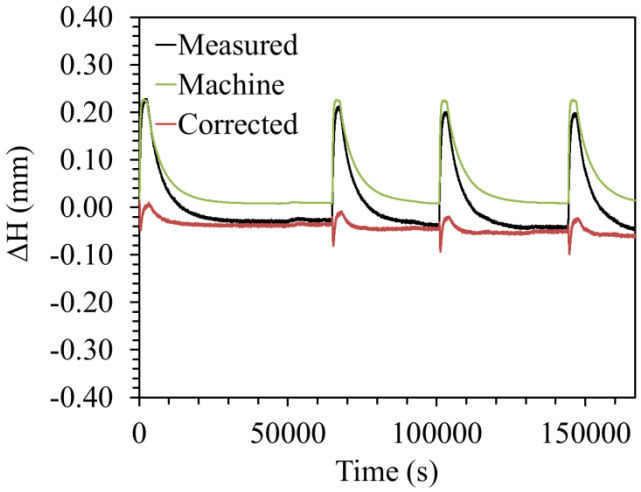

Figure 6.15: Change in height versus time for the OCR 1.67 test

Table 6.4: Summary of results for OCR 1.67 test

Temperature Cycle	Heating rate (°C/min)		Initial temperature (°C)	Final temperature (°C)		ΔH (mm)		
	Target	Measured		Target	Measured	Start of Heating	End of Heating	End of Cooling
1	1.00	1.74	15.70	90	91.09	0.000	-0.002	0.036
2	1.00	1.72	18.65	90	91.08	0.033	0.014	0.046
3	1.00	1.70	18.40	90	90.67	0.044	0.025	0.049
4	1.00	1.61	18.56	90	90.94	0.050	0.026	0.068

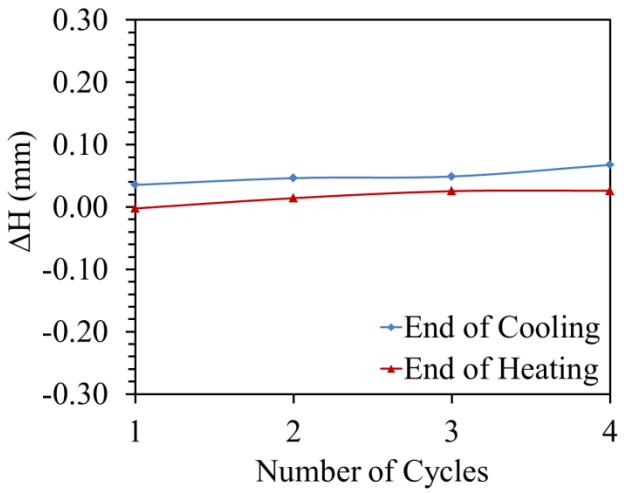

Figure 6.16: Variations in deflections with temperature cycles for the OCR 1.67 test

6.5. OCR 5.00 Test

This test was performed to evaluate the changes in volume of an over consolidated (OCR=5.00) compacted silt specimen during four cycles of heating and cooling. Before thermal loading, the specimen was mechanically loaded in an isothermal consolidation test to 1310 kPa and then unloaded to 262 kPa, giving an overconsolidation ratio (OCR) of 5.00. Once isothermal consolidation was complete, the specimen was heated from the ambient room temperature to 90°C in a single rapid heating step at rate of 3.0°C/min. This first heat cycle was followed by unassisted cooling to room temperature by turning by turning off the heat source. Each subsequent temperature cycle was conducted by applying the same rates of fast heating to the silt followed by unassisted cooling to room temperature. The curve in Figure 6.17 represents the heating and cooling paths followed in the OCR 5.00 test. The thermal consolidation test was conducted at the end of the isothermal consolidation test under an effective stress of 262 kPa, which was held constant. The vertical effective stress measured by the load cell throughout the test period is shown in Figure 6.18.

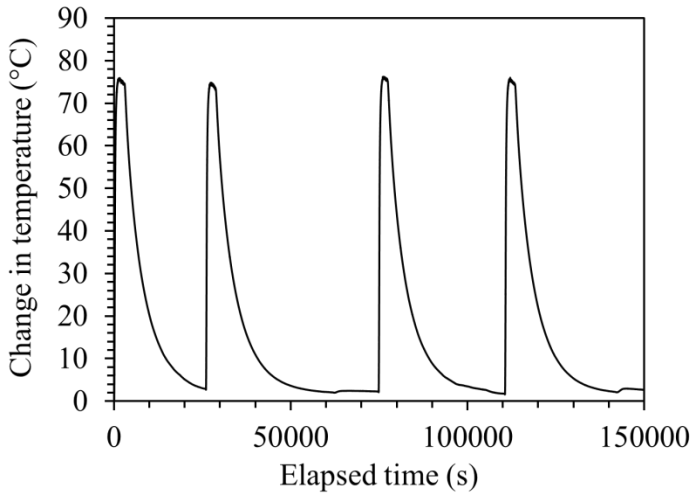

Figure 6.17: Temperature versus time for the OCR 5.00 test

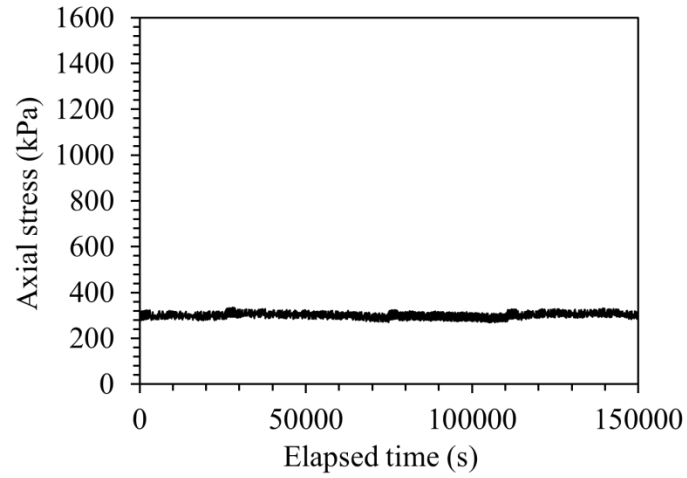

Figure 6.18: Axial stress versus time for the OCR 5.00 test

The excess pore water pressures generated during each heating cycle was measured using pore pressure and differential pressure transducers. The corresponding excess pore water pressure generated during heating cycles measured by the pore pressure and differential pressure transducers is shown if Figure 6.19. Consistent with the trends observed for the two previous overconsolidated specimens, there were small decreasing magnitudes of excess pore water pressure generated through each heating cycle. It is observed that the measured deflections in Figure 6.20 also respond with contractive response after the first heating cycle and each

temperature cycle that followed produced little to no deflection. These results are summarized in Table 6.5 and. The table contains the initial and final values of the measured temperatures, rates of heating, and deflections for each temperature cycle. The cycle versus deflection plot in Figure 6.21 further reflects that there is almost no change in the height of the specimen after the test is completed.

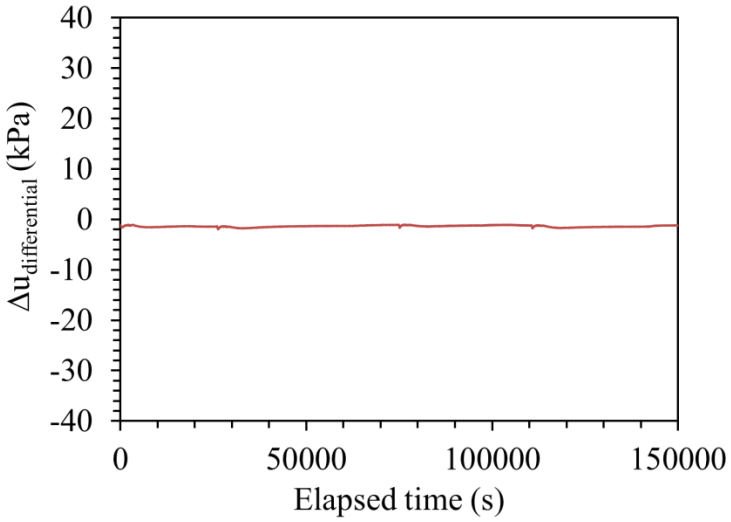

Figure 6.19: Changes in thermally induced pore water pressure measured by the DPT versus time for the OCR 5.00 test

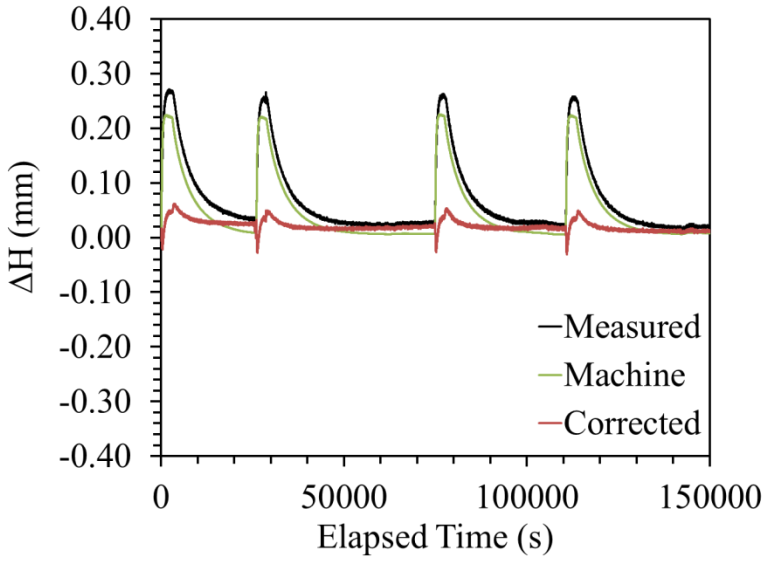

Figure 6.20: Change in height versus time for the OCR 5.00 test

Table 6.5: Summary of results for the OCR 5.00 test

Temperature Cycle	Heating rate (°C/min)		Initial temperature (°C)	Final temperature (°C)		ΔH (mm)		
	Target	Measured		Target	Measured	Start of Heating	End of Heating	End of Cooling
1	1.00	1.60	16.406287	90	91.06658	0.000	-0.046	-0.011
2	1.00	1.57	19.246647	90	89.82793	-0.012	-0.038	-0.022
3	1.00	0.64	18.669207	90	91.67324	-0.021	-0.036	-0.017
4	1.00	1.11	18.152321	90	90.74676	-0.017	-0.033	-0.011

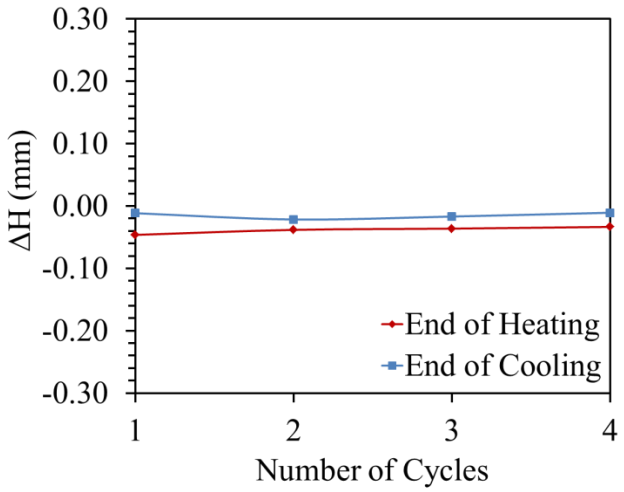

Figure 6.21: Variations in deflections with temperature cycles for the OCR 5.00 test

6.6. OCR 10.00 Test

This test was performed to evaluate the changes in volume of an over consolidated (OCR=10.00) compacted silt specimen during four cycles of heating and cooling. Before thermal loading, the specimen was mechanically loaded in an isothermal consolidation test to 1310 kPa and then unloaded to 131 kPa, which resulted in an overconsolidation ratio (OCR) of 10.0. Once isothermal consolidation was complete, the specimen was heated from the ambient room temperature to 90°C in a single rapid heating step at rate of 3.0°C/min. This first heat cycle was followed by unassisted cooling to room temperature by turning by turning off the heat source. Each subsequent temperature cycle was conducted by applying the same rates of fast heating to

the silt followed by unassisted cooling to room temperature. The curve in Figure 6.22 represents the heating and cooling paths followed in the OCR 1.67 test. The thermal consolidation test was conducted at the end of the isothermal consolidation test under an effective stress of 131 kPa, which was held constant. The vertical effective stress measured by the load cell throughout the test period is shown in Figure 6.23.

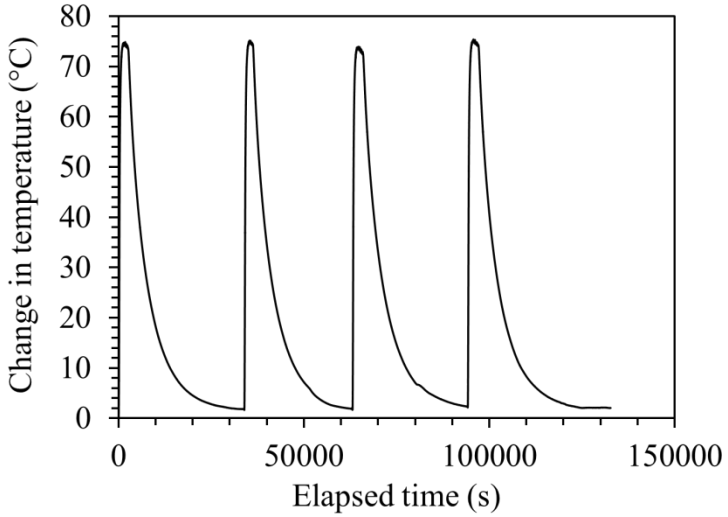

Figure 6.22: Temperature versus time for the OCR 10.0 test

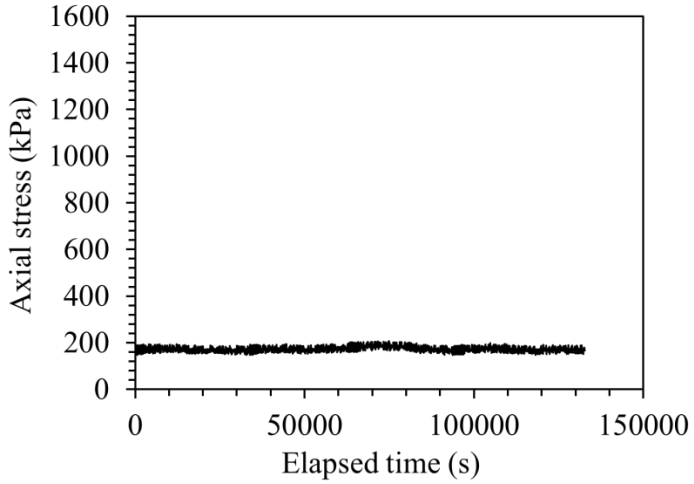

Figure 6.23: Axial stress versus time for the OCR 10.0 test

The excess pore water pressures generated during each heating cycle was measured using pore pressure and differential pressure transducers. The corresponding excess pore water pressure generated during heating cycles measured by the pore pressure and differential pressure

transducers is shown if Figure 6.24. The DPT measurements show a small magnitude of thermally induced pore water pressure consistent with the other overconsolidated specimens.

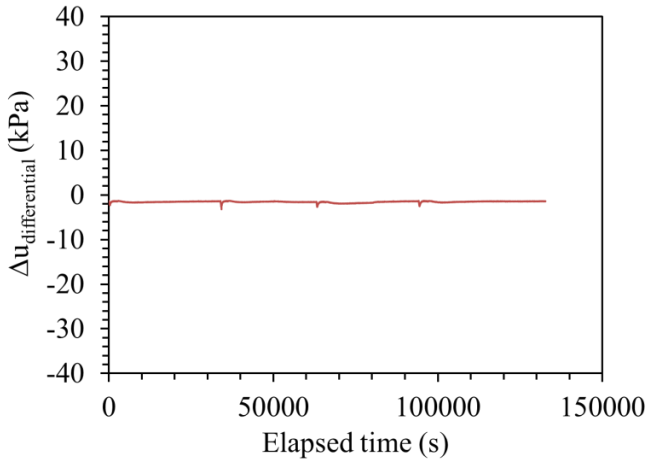

Figure 6.24: Changes in thermally induced pore water pressure measured by the DPT versus time for the OCR 10.0 test

Figure 6.25 shows the deflections for the OCR 10.00 test. Following the four previous observations, the response of the silt was expansive immediately following the first heating cycle. The results in Figure 6.26 indicate that the remaining thermal cycles show inconsistent trends. These results are summarized in Table 6.6. The table contains the initial and final values of the measured temperatures, rates of heating, and deflections for each temperature cycle.

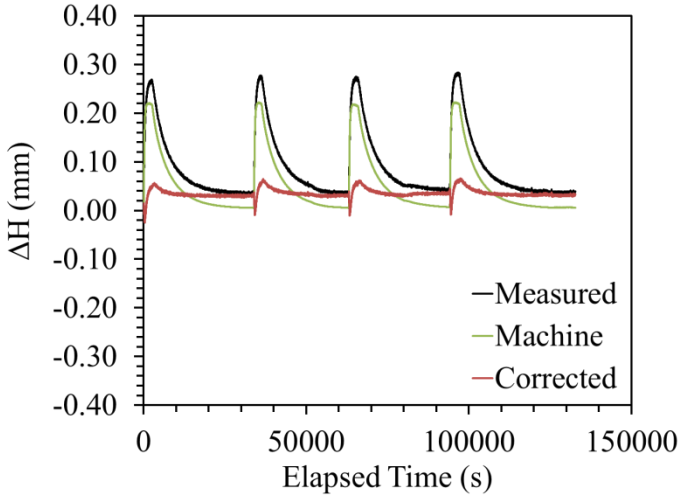

Figure 6.25: Change in height versus time for the OCR 10.0 test

Table 6.6: Summary of results for the OCR 10.0 test

Temperature Cycle	Heating rate (°C/min)		Initial temperature (°C)	Final temperature (°C)		ΔH (mm)		
	Target	Measured		Target	Measured	Start of Heating	End of Heating	End of Cooling
1	1.00	1.72	16.859186	90	90.56665	0.000	-0.050	-0.030
2	1.00	1.89	18.673006	90	91.22467	-0.028	-0.055	-0.030
3	1.00	1.50	18.718603	90	89.43842	-0.030	-0.055	-0.036
4	1.00	1.50	19.163087	90	91.04085	-0.034	-0.061	-0.033

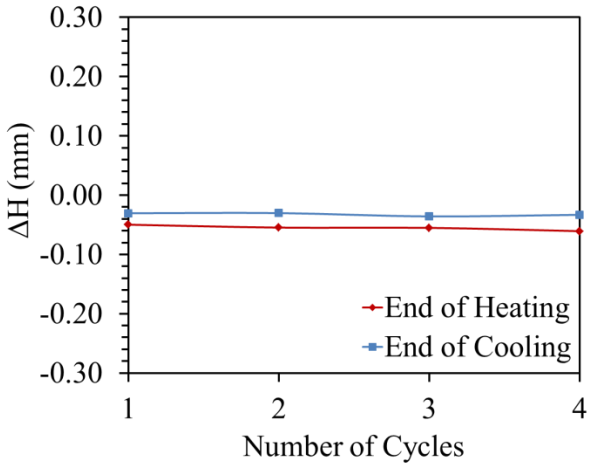

Figure 6.26: Variations in deflections with temperature cycles for the OCR 10.0 test

7. ANALYSIS

7.1 Temperature-Strain Behavior

The common approach for analyzing the thermal compression behavior of soils is to develop plots of thermal axial strain versus the change in temperature. The slope of this line is equal to the coefficient of thermal expansion of the soil skeleton under drained conditions. The results for the normally consolidated (OCR = 1) silt specimen are shown in Figure 7.1. The results in this figure indicate that the specimen contracted during the first heating cycle as expected. Instead of following the same slope as the cooling strains, the strain bowed outwards to the right during heating on each subsequent stage. The slopes of the strain data during each cooling stages are all consistent. The hysteresis loops in this figure may be due to the radial ring-soil interaction during heating and cooling, and a further in-depth heat flow analysis is needed to interpret these results. A summary of the thermal volume change at the end of the heating and cooling phases is shown in Figure 7.2. These results show a steady increase in permanent strain after each cooling cycle. It is rare to encounter normally consolidated soils in the regions in which energy foundations are typically installed, but these results indicate that further research is needed to quantify this behavior in a constitutive model.

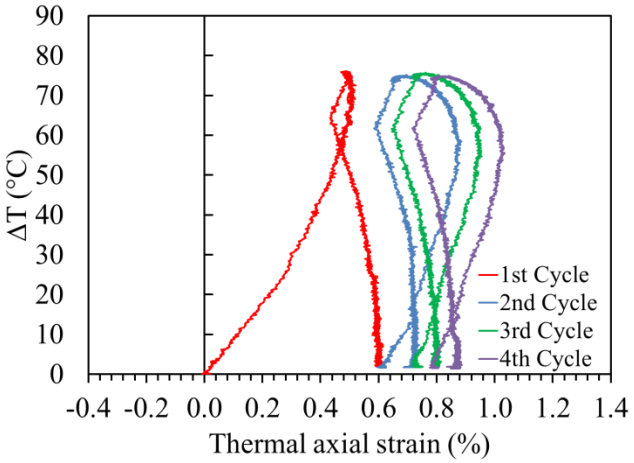

Figure 7.1: Temperature-axial strain plot for saturated silt with OCR = 1

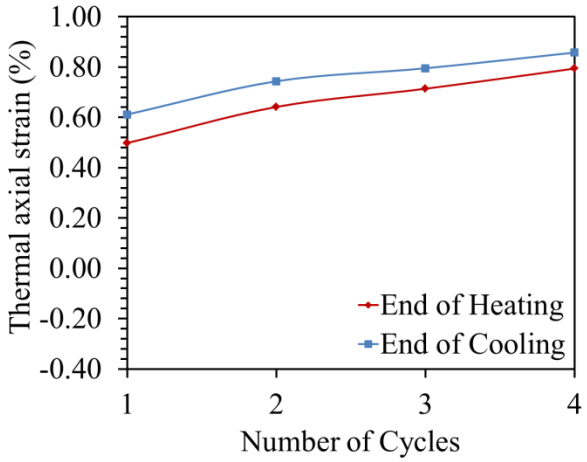

Figure 7.2: Cyclic changes in thermal axial strain after the end of heating and cooling for saturated silt with OCR = 1

The results for the silt specimen with an OCR of 1.25 are shown in Figure 7.3. Different from the normally consolidated specimen, a slight expansion is noted during the first heating cycle. However, similar to the normally consolidated specimen, continued contraction is observed after each cooling cycle. These results are confirmed by the steady increasing trend in permanent axial strains after each heating cycle shown in Figure 7.4.

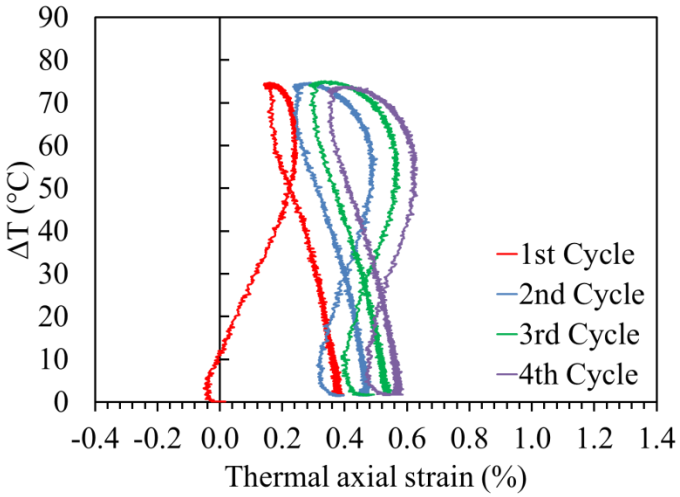

Figure 7.3: Temperature-axial strain plot for saturated silt with OCR = 1.25

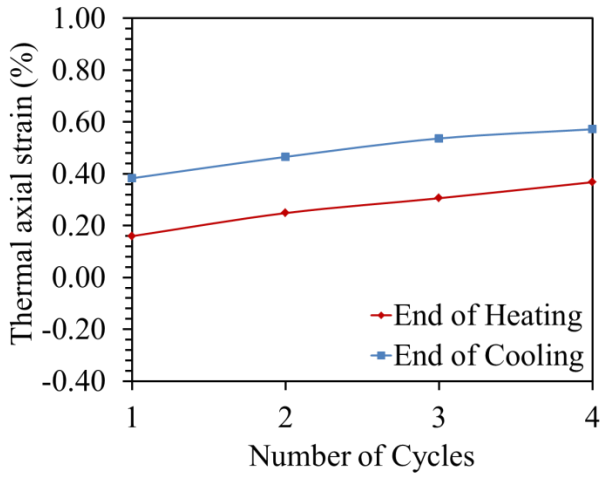

Figure 7.4: Cyclic changes in thermal axial strain after the end of heating and cooling for saturated silt with OCR = 1.25

The results for the silt specimen with an OCR of 1.67 are shown in Figure 7.5. Different from the specimen with OCR = 1.25, a more substantial expansion is noted during the first heating cycle. Less contraction is noted during each subsequent heating-cooling cycle. These results are confirmed by the nearly flat trend in permanent axial strains after each heating cycle shown in Figure 7.6.

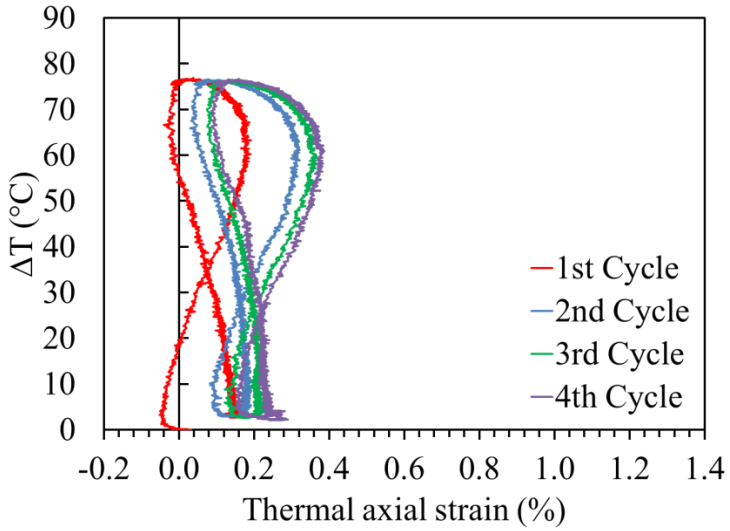

Figure 7.5: Temperature-axial strain plot for saturated silt with OCR = 1.67

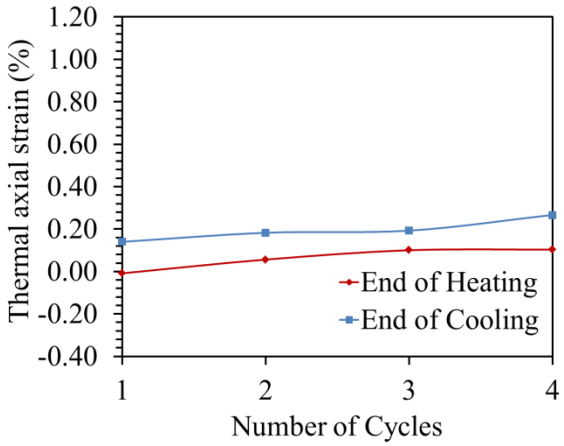

Figure 7.6: Cyclic changes in thermal axial strain after the end of heating and cooling for saturated silt with OCR = 1.67

The results for the silt specimen with an OCR of 5.0 are shown in Figure 7.7. Similar to the specimen with OCR = 1.67, the specimen expanded elastically during the first heating cycle, and did not show any additional permanent axial strains after each heating-cooling cycle. These results are confirmed by the nearly flat trend in permanent axial strains after each heating cycle shown in Figure 7.8.

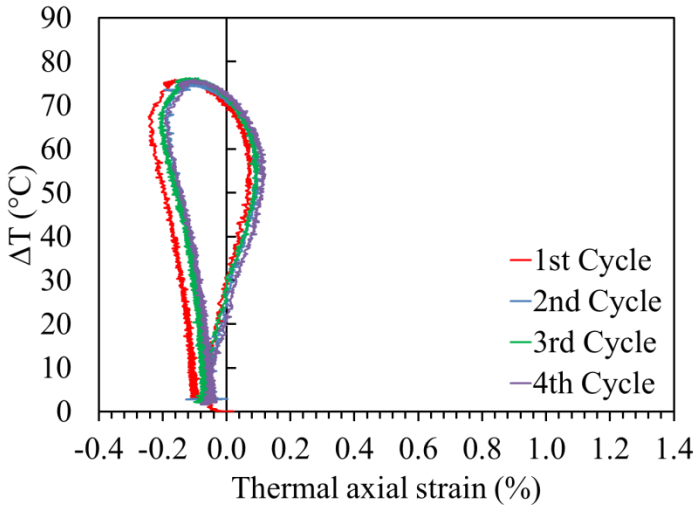

Figure 7.7: Temperature-axial strain plots for saturated silt with OCR = 5.0

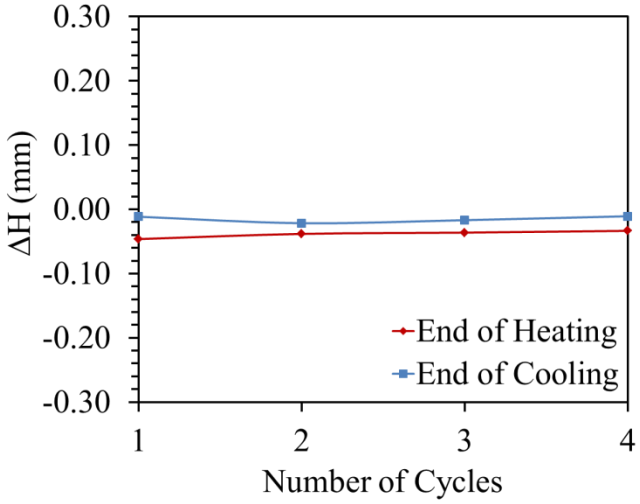

Figure 7.8: Cyclic changes in thermal axial strain after the end of heating and cooling for saturated silt with OCR = 5.0

The results for the silt specimen with an OCR of 10.0 are shown in Figure 7.9. Similar to the specimen with OCR = 1.67 and 5.0, the specimen expanded elastically during the first heating cycle. A slight amount of thermal contraction was observed during subsequent heating-cooling cycles, but not as significant as in the tests with OCR = 1 and 1.25, as shown in Figure 7.10.

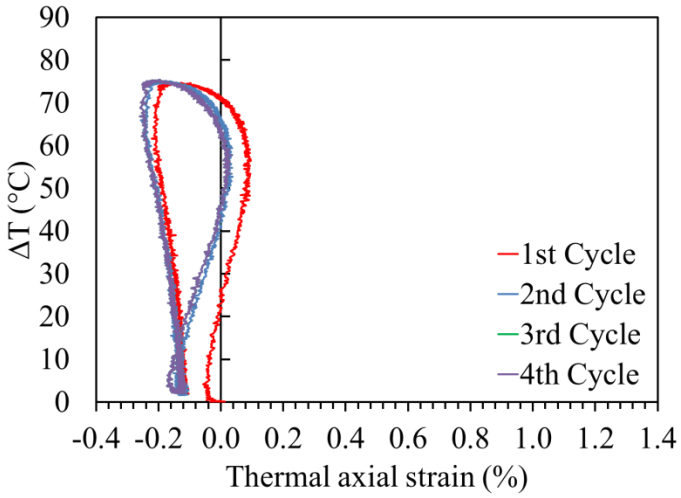

Figure 7.9: Temperature-axial strain plots for saturated silt with OCR = 10

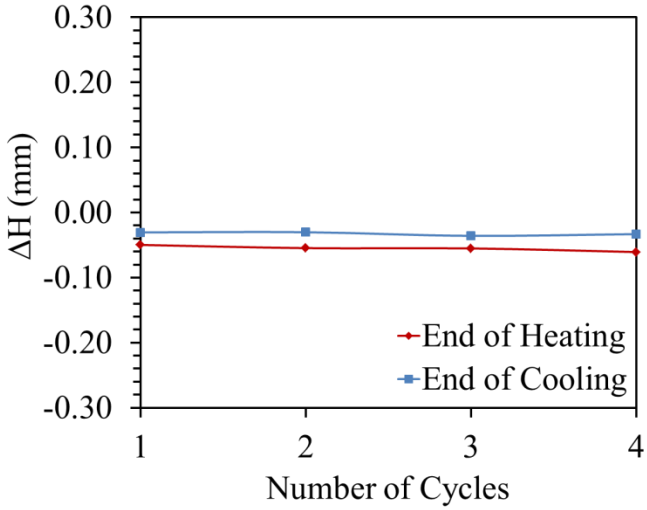

Figure 7.10: Cyclic changes in thermal axial strain after the end of heating and cooling for saturated silt with OCR = 10.0

A summary of the permanent thermal axial strains during cooling for each of the silt specimens having different OCR values is shown in Figure 7.11(a). The slopes of these lines as a function of OCR are shown in Figure 7.11(b). The decreasing slope with increasing OCR indicates that the greater the OCR, the less impact that continued thermal cycling will have on the thermal volume change of a soil layer. As energy foundations are primarily used in overconsolidated soil deposits, this is a positive conclusion.

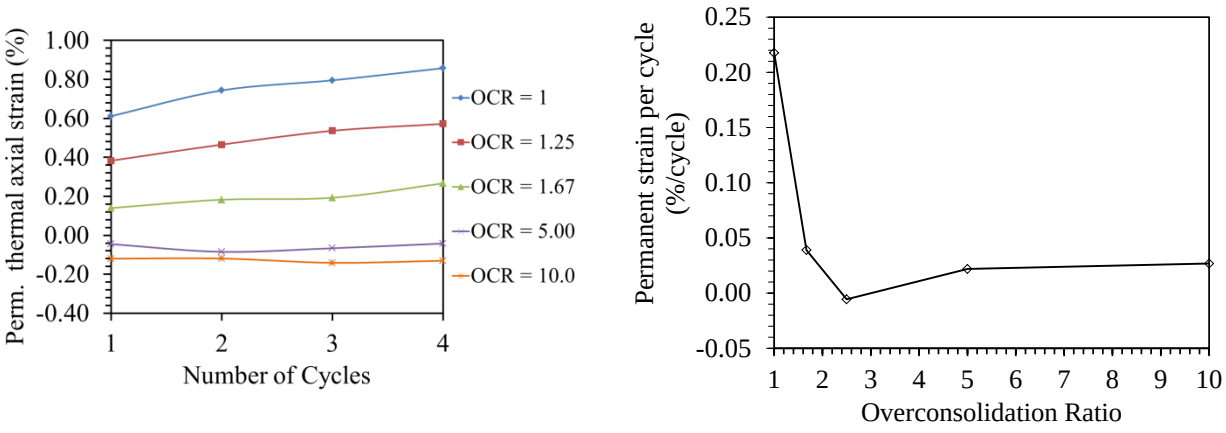

(a) (b)

Figure 7.11: Summary of results: (a) Permanent thermal volume change after cooling as a function of cooling for specimens with different OCR values; (b) Slope of the cyclic thermal volume change trends as a function of OCR

7.2 Temperature-Pore Water Pressure Behavior

The change in thermally induced pore water pressure as a function of temperature cycles is shown in Figure 7.12. This plot indicates that positive thermally induced pore water pressures are generated during each heating cycle of the tests on the normally consolidated soil. For the overconsolidated soils, the thermally induced pore water pressures are relatively constant on each cycle. There is no clear trend with OCR although the magnitude of thermally induced pore water pressure is small compared to that of the normally consolidated soil. It is possible that the slight difference in void ratios at the beginning of thermal consolidation led to the variability noted in this figure.

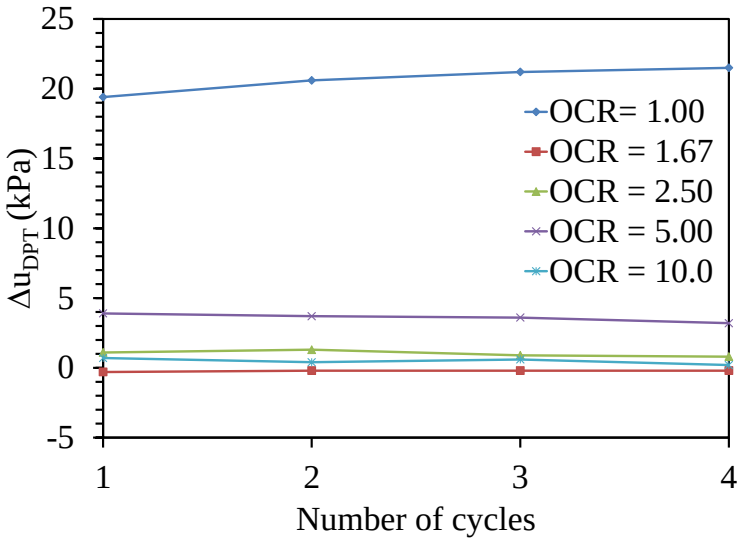

Figure 7.12: Summary of thermally induced pore water pressures during heating from 20 to 90 °C as a function of temperature cycles for the specimens with different OCR values

8. CONCLUSIONS

A series of five thermal consolidation tests were performed on saturated silt specimens having different initial stress states with a thermal oedometer having single-drainage boundary conditions. In each test, four cycles of heating and cooling from room temperature (20 °C) to approximately 90 °C and back were applied, during which changes in axial deformation and pore water pressure response were measured. The following conclusions can be drawn from this study:

- During the first heating phase, the normally consolidated silt specimens were observed to show permanent contraction while the overconsolidated silt specimens were observed to show expansion.
- During the subsequent cooling phase, all specimens were observed to show elastic contraction.
- During additional heating and cooling phases, the specimens all showed a small amount of additional contraction, regardless of the stress state. The normally consolidated specimen showed the greatest amount of additional permanent contraction.
- Changes in pore water pressure were noted during each heating cycle for the normally consolidated specimen, supporting the axial deformation results which indicate that continued permanent contraction occurs during each heating and cooling cycle. Specimens with a greater overconsolidation ratio show less pore water pressure generation during heating.
- The machine deformations were observed to have an important role on the final thermal volume change results, indicating that this is a critical variable to measure in future testing.

- The results from this study provide data which is useful to further refine the fundamental response of thermo-elasto-plastic models for unsaturated soils. Specifically, because an increase in pore water pressure was observed at the beginning of each heating cycle, albeit with a smaller magnitude than the previous cycle, a hardening law which retains some memory of the previous heating cycle, but not all, may be a useful approach.

REFERENCES

Abdel-Hadi, O.N., and Mitchell, J.K. 1981. "Coupled heat and water flows around buried cables." Journal of the Geotechnical Engineering Division, ASCE. 107(11): 1461–1487.

Baldi, G., Hueckel, T., and Pellegrini, R. 1988. "Thermal volume changes of the mineral-water system in low-porosity clay soils." Canadian Geotechnical Journal, 25: 807–825.

Baldi, G., Hueckel, T., Peano, A., Pellegrini, R. 1991. Developments in Modelling of Thermo-Hydro-Geomechanical Behaviour of Boom clay and Clay-Based Buffer Materials. Report to the Commission of the European Communities. Nuclear Science and Technology EUR 13365/2.

Brandl, H. 2006. "Energy Foundations and other Thermo-Active Ground Structures." Géotechnique. 56(2), 81-122.

Burghinoli, A. Desideri, A. and Miliziano, S. 1992. "Deformability of clays under non-isothermal conditions." Revista Italiana di Geotechnica. 4/92, 227-236.

Burghignoli A., Desideri A., and Miliziano S. 2000. "A laboratory study on the thermomechanical behaviour of clayey soils." Canadian Geotechnical Journal. 37: 764-780.

Campanella, R.G., and Mitchell, J.K. 1968. "Influence of temperature variations on soil behavior." Journal of the Soil Mechanics and Foundation Engineering Division, ASCE, 94(SM3): 709–734.

Cekerevac, C., and Laloui, L. 2004. "Experimental study of thermal effects on the mechanical behavior of a clay." International Journal for Numerical Analytical Methods Geomechanics, 28: 209–228.

Demars, K. R., and Charles, R. D. 1982. "Soil volume changes induced by temperature cycling." Canadian Geotechnical Journal. 19: 188–194.

El Tawati, A. (2010). Impact of the Rate of Heating on the Thermal Consolidation of Compacted Silt. M.S. Thesis. University of Colorado Boulder.

Finn, F. N. 1951. "The effects of temperature on the consolidation characteristics of remolded clay." Symposium on Consolidation Testing of Soils, ASTM, Special Technical Publication, No. 126: 65–72.

Gray, H. 1936. "Progress report on the consolidation of fine-grained soils." *In* Proc. of the 1st Int. Conf. on Soil Mechanics and Foundation Engineering, Cambridge, Mass., 138–141.

Hillel, D. 1998. Environmental Soil Physics. Academic Press, San Diego, California, p. 49.

Hueckel, T., and Baldi, M. 1990. "Thermoplasticity of saturated clays: experimental constitutive study." Journal of Geotechnical Engineering, 116(12): 1778–1796.

Hueckel, T. and Borsetto, M. 1990. "Thermoplasticity of saturated soils and shales: Constitutive equations." Journal of Geotechnical Engineering. 116(12): 1765-1777.

Lamond, J.F., and Pielert, J.H., ed. 2006. Significance of Tests and Properties of Concrete and Concrete-Making Materials. ASTM International, New Jersey, p. 426.

Lide, D.R., ed. 2010. CRC Handbook of Chemistry and Physics, 90th Edition (Internet Version), CRC Press/Taylor and Francis, Boca Raton, Florida, p. 6-140.

McGinley, J.M. 1983. The Effects of Temperature on the Consolidation Process of Saturated Fine-Grained Soils. M.S. Thesis, Department of Civil, Environmental and Architectural Engineering, University of Colorado, Boulder, Colorado.

McKinstry, H.A. 1965. "Thermal expansion of clay minerals." The American Mineralogist, 50: 212–222.

Mitchell, J.K., and Soga, K. 2005. Fundamentals of soil behavior. John Wiley & Sons, Inc., 3rd ed., New Jersey.

Murphy, K. and McCartney, J.S. 2012. "Full-Scale Performance of Energy Foundations in Colorado." GeoChallenges 2012. November 9th, 2012. Lakewood, CO. ASCE.

Omer, A.M. 2008. "Ground-source heat pumps systems and applications." Renewable and Sustainable Energy Reviews. 12(2), 344-371.

Rosenberg, J.E. 2010. Centrifuge Modeling of Soil Structure Interaction in Geothermal Foundations. MS Thesis. University of Colorado Boulder.

Passwell, R.E. 1967. "Temperature effects on clay soil consolidation." Journal of the Soil Mechanics and Foundation Engineering Division, ASCE, 93(SM3): 9–22.

Plum, R.L., and Esrig, M.I. 1969. "Some temperature effects on soil compressibility and pore water pressure." *In* Effects of temperature and heat on engineering behavior of soils. Highway Research Board, Washington, DC. Special Report, No. 103: 231–242.

Slegel, D.L., and Davis, L.R. 1977. "Transient heat and mass transfer in soils in the vicinity of heated porous pipes." Journal of Heat Transfer, 99: 541–621.

Stewart, M.E. 2012. Centrifuge Modeling of Strain Distributions in Energy Foundations. MS Thesis. University of Colorado Boulder.

Sultan, N., Delage, P., and Cui, Y.-J. 2002. "Temperature effects on the volume change behavior of Boom clay." Engineering Geology, 64: 135–145.

Tidfors, M., and Sällfors, G. 1989. "Temperature effect on preconsolidation stress." Geotechnical Testing Journal, 12(1): 93–97.

Towhata, I., Kuntiwattanakul, P., Seko, I., and Ohishi, K. 1993. “Volume change of clays induced by heating as observed in consolidation tests.” Soils and Foundations, 33(4): 170–183.

Vega, A., Coccia, C.J.R., El Tawati, A. and McCartney, J.S. 2012. “Impact of the Rate of Heating on the Thermal Consolidation of Saturated Silt.” ASCE GeoCongress 2012. Oakland, CA. March 25-29th 2012. 10 pg.